Journal Pre-proof

Comparison of fold-thrust belts driven by plate convergence and gravitational failure

Xiaodong Yang, Frank J. Peel, Lisa C. McNeill, David J. Sanderson

PII: S0012-8252(19)30742-1

DOI: https://doi.org/10.1016/j.earscirev.2020.103136

Reference: EARTH 103136

To appear in: *Earth-Science Reviews*

Received date: 6 November 2019

Revised date: 14 February 2020

Accepted date: 14 February 2020

Please cite this article as: X. Yang, F.J. Peel, L.C. McNeill, et al., Comparison of fold-thrust belts driven by plate convergence and gravitational failure, *Earth-Science Reviews*(2020), https://doi.org/10.1016/j.earscirev.2020.103136

This is a PDF file of an article that has undergone enhancements after acceptance, such as the addition of a cover page and metadata, and formatting for readability, but it is not yet the definitive version of record. This version will undergo additional copyediting, typesetting and review before it is published in its final form, but we are providing this version to give early visibility of the article. Please note that, during the production process, errors may be discovered which could affect the content, and all legal disclaimers that apply to the journal pertain.

© 2020 Published by Elsevier.

Journal Pre-proof

Comparison of Fold-Thrust Belts Driven by Plate Convergence and Gravitational Failure

Xiaodong Yang[1,*,#], Frank J. Peel[2,3], Lisa C. McNeill[1], David J. Sanderson[1]

[1] School of Ocean and Earth Science, National Oceanography Centre Southampton, University of Southampton, Southampton, SO14 3ZH, UK.

[2] Department of Earth Science and Engineering, Imperial College London, London, SW7 2BP, UK.

[3] Bureau of Economic Geology, The University of Texas at Austin, Austin, TX, USA

*Corresponding author, email: yang@ipgp.fr

Now at Laboratoire de Geoscience Marine, Institut de Physique du Globe de Paris, 1 rue Jussieu, 75238 Paris Cedex 05, France.

Journal Pre-proof

Abstract

Submarine Fold-thrust belts (FTBs) are predominantly formed by the deformation of sedimentary sequences as a result of subduction of oceanic plates at active margins, gravitational failure at many passive margins, or a combination of these two at both types of margin. A key question is: Is the FTB driven by gravitational failure basically the same as the FTB driven by plate convergence or are there fundamental differences? Deepwater FTBs in the toes of gravity-driven systems display many elements of structural style that are similar or even identical to those in FTBs driven by plate convergence. However, some structural elements and elements of fold-thrust belt development history differ between the two systems.

To address this, we used examples from various tectonic settings (end members and hybrid systems) to conduct detailed structural analysis in terms of geometry, structure, strain distribution, shortening rate, deformation history, and tectonic process. The new results suggest: (1) The energy source in gravity-driven systems is the gravitational potential energy within the sedimentary material itself that is being deformed to create the updip extension and downdip contraction, whereas it is the movement of stressed lithospheric-scale tectonic plates, which lie outside the local sediment pile and within the

broader undeformed crust and lithosphere; (2) as a result, the thickening is attained largely by deposition of the syn-kinematic sequence in the gravity-driven system, whereas it is attained by shortening and stratigraphic repetition by thrusting in the plate convergence-driven system; (3) the energy in gravity-driven systems is resupplied by sediment input from large river deltas and therefore deformation tends to be episodic, linked to major episodes of sediment input. Whereas in a system driven by plate motions, the energy is resupplied by movement of a boundary upon which force is acting, and tends to be continuous, and less episodic; (3) the thrust faults of both systems are predominantly basinward-verging thrust faults. Backthrusts and back rotation appear to be only observed in the purely or predominantly plate convergence driven systems; 4) the rate of shortening across plate convergence-driven systems is high (e.g. 43-48mm/yr in Hikurangi, 37-46 mm/yr in the Makran), and generally continuous on a long timescale. Whereas across the contractional domain of gravity-driven systems, shortening is slow (e.g. 1.4-2.0 mm/yr in the Niger delta, 0.8 mm/yr in the Para-Maranhao basin) and more variable through time; (5) for both driving mechanisms, the fold-thrust belt propagates forward with new thrust initiation at the toe, but fault activity differs slightly. Focused activity at the toe of the FTB is more common where driven by plate convergence but not observed in gravity-driven systems. Activity across much of the FTB is observed for both systems, but activity focused in the rear to middle of the FTB is only observed in gravity-driven systems; (6) the plate-driven system is primarily limited by rate of plate motion, i.e., the rate at which the plate is fed into the FTB, whereas in a system driven by gravity, the movement is limited (resisted) by the strength of the sediments and detachment.

Key words: gravitational failure; plate convergence; fold-thrust belt; thrust faults; structural propagation; strain distribution; shortening rates.

1. Introduction

Three main tectonic settings that can host Fold-Thrust Belts (FTBs) are: (1) subduction zones associated with oceanic-continental or oceanic-oceanic plate convergence at active margins, in the form of submarine accretionary wedges (Fig. 1*a*) (Davis et al., 1983; Moore and Silver, 1987; von Huene and Scholl, 1991), (2) the subaerial foreland of orogeny associated with continent-continent collision or intracontinental shortening (e.g. Rodgers, 1949; Coward, 1983; Buiter, 2012) and (3) the contractional toes of gravity-driven linked systems of extension and contraction, most commonly developed on

passive continental margins where the sediment sequence lies above a weak décollement (salt, overpressured mud or shale) (e.g. Rowan et al., 2004; Hamilton and De Vera, 2009; Butler and Paton, 2010; Butler and Turner, 2010; Morley et al., 2011; Wu et al., 2015; Scarselli et al., 2016; King and Morley, 2017) (Fig. 1b). Note that FTBs may have components of both plate convergence and gravitational deformation, creating hybrid systems, such as the Makran accretionary prism (Grando and McClay, 2007; Smith et al., 2012), the Cascadia (Washington) margin (McNeill et al., 1997), the NW Borneo FTB (e.g. Hinz et al., 1989; Ingram et al., 2004; Morley, 2007; Hesse et al., 2009; King et al., 2010b).

Understanding of the geometry and processes of FTBs began with the study of onshore fold belts that were driven by continent-continent collision, such as the Scottish Moine Thrust Belt (Peach et al., 1907), the Canadian Rockies and the Alps (e.g. Bally et al., 1966; Dahlstrom, 1969; Dahlstrom, 1970; Price and Mountjoy, 1970). This setting dominated our paradigm of FTBs to such an extent that the classic paper of Boyer and Elliott (1982) entitled "Thrust Systems" makes no mention of any other context.

From the 1970s onwards, largely through the use of marine 2D reflection data, information on accretionary wedges in zones of oceanic subduction emerged, revealing that these consist of thrust systems with close relation to onshore FTBs (e.g. Westbrook, 1975; Von Huene, 1979; Moore and Curray, 1980). Continuing study of accretionary wedge systems, motivated in part by the need to assess geohazard potential including earthquakes, tsunamis and landslides through understanding of properties of the underlying plate boundary (e.g. Westbrook et al., 1982; White, 1982; White and Louden, 1982; Moore and Silver, 1987; Westbrook et al., 1988; Moore et al., 1990; Morgan and Karig, 1995), has confirmed that accretionary systems form a continuum with FTBs in continental collision settings.

Information on a different class of FTB began to emerge in the 1990s, spurred on by the move of petroleum exploration into progressively deeper water on passive continental margins. These deepwater passive margin toe-thrust belts in gravity-driven linked systems were initially identified on 2D reflection seismic data, and later supported by 3D seismic data and exploration drilling. The first published examples came from the US Gulf of Mexico (e.g. Wu et al., 1990; Weimer and Buffler, 1992; Diegel et al., 1995; Peel et al., 1995; Trudgill et al., 1995; Trudgill et al., 1999; Rowan et al., 2000). Examples from other basins have subsequently been published, e.g. Niger Delta, Orange Basin and offshore

Brazil (Rowan et al., 2004; Bilotti and Shaw, 2005; Corredor et al., 2005; Granado et al., 2009; Morley et al., 2011; Cruciani and Barchi, 2016; Scarselli et al., 2016; Cruciani et al., 2017). As data emerges across the world, it appears that gravity-driven FTB systems may develop in all passive margins where a major source of clastic sediments feeds onto a margin that includes a potential detachment surface.

A key question is: Is this new class of FTB basically the same as the FTBs driven by plate convergence or are there fundamental differences? Deepwater FTBs in the toes of gravity-driven linked systems on passive margins display many elements of structural style that are similar, or even identical, to those seen in FTBs driven by plate convergence. However, some structural style elements or elements of fold-thrust belt development history may differ between FTBs driven by plate convergence and gravity.

Here we compare examples of FTBs from gravity-driven systems and from systems driven by plate convergence to document similarities and differences in structural style and tectonic evolution. We examine whether the difference in tectonic setting and the different boundary conditions, may give rise to differences in structure, behaviour and evolution.

Morley et al. (2011) argued that that dividing FTB systems into gravity-driven and plate-convergence-driven cases does not encompass all types of offshore FTB, and proposed a more complex classification based on the driving mechanism, tectonic setting, and detachment type. However, this classification appears to be too specific with many sub-types, affecting the structural comparison between them. Here we choose to use the conventional classification, simplified as gravity-driven, plate convergence-driven, or a hybrid system.

Despite significant similarities between gravity-driven and plate convergence-driven FTBs, such as wedge shape, fold and thrust structure/geometry, presence of large-scale horizontal shortening (Rowan et al., 2004; Morley et al., 2011), there are significant differences in mechanism and deformation.

In a plate convergence-driven system:

1. The convergence zone lies within a system whose boundary surfaces are moving, and upon those bounding surfaces, forces are acting in the form of plate-scale stress fields. Therefore energy sourced from plate motion is continually fed into the system.

Journal Pre-proof

2. Naturally, body forces (in the form of gravity) act upon the zone of convergent deformation. They play a significant part in controlling the local tectonic processes within the zone, but do not provide the energy to power them.
3. The rate of plate convergence is governed by global plate motions with relatively stable long-term rate of convergence that is independent of the geometry and strength of the deforming wedge and basal detachment. The system will not stop if these conditions become unfavourable to easy deformation.

In a gravity-driven system:

1. The FTB lies within a system whose boundary surfaces are not moving relative to one another. Therefore no energy is fed into the system across the bounding surfaces.
2. Body forces (in the form of gravity) act upon the region of deformation. In addition to playing a significant part in controlling the local tectonic processes within that zone, these forces provide the energy that powers them (Peel, 2014).
3. The rate of tectonic contraction is governed by the dynamics of local gravitational failure, it is therefore dependent on the geometry and strength of the deforming system and basal décollement. The system may stop, or indeed may never start, if these conditions are unfavourable.

In a hybrid system:

1. The shortening at the toe of the system is driven by both plate convergence and by updip extension that may act contemporaneously or separately. The relative role of each is likely to vary between hybrid systems and through time.
2. Energy is fed into the system by body forces and by movement of the boundaries.

To investigate the impacts of the differences in driving mechanisms, seismic reflection data are used here to carry out the in-depth examinations of multiple (8) examples of FTBs from a range of end member and hybrid systems (Fig. 2). We note that submarine FTBs are better imaged due to seismic imaging than their subaerial counterparts (Butler and Paton, 2010). This paper is the first detailed study of the differences and similarities in terms of driving mechanisms, geometries, structural styles and tectonic history. Specifically, we (1) describe the geometry of the structures, (2) examine the interaction of the structures involved in the system, i.e. folds, faults and basal detachment, (3) investigate the timing of deformation within and between the contractional and

Journal Pre-proof

extensional parts of the systems, (4) quantify the strain distribution and partitioning in the system, and (5) explore the tectonic and mechanical control on the FTBs.

2. Workflow

Key methods used in this study are seismic interpretation, tectono-stratigraphic mapping, structural analysis, strain measurement and deformation quantification. The FTB examples were selected for the quality of their seismic datasets, imaging of seismic stratigraphy and deformation, and prior interpretative studies. To apply the methods, we developed a simple workflow: (1) map the stratigraphic units in a cross-section of FTBs based primarily on previous interpretations; (2) identify the deformation-related sedimentary successions, i.e. basement, pre-kinematic, syn-kinematic and post-kinematic, based on the relationship between structural development (thrusting, folding and uplifting) and depositional timing (growth strata), (3) group the different types of fault, i.e. normal fault, detachment fault, basinward/seaward-vergent thrust fault and/or landward-vergent thrust fault; (4) analyse the timing of folding and faulting of individual structures in a system; (6) quantify the amount of contraction, extension or both, as relevant, as a proxy for strain distribution and partitioning in examples with well-imaged stratigraphy and displacement; and (5) evaluate the deformation initiation and propagation location, timing and patterns. We map these different tectono-stratigraphic elements consistently between examples. The same colour scheme is used in all examples to highlight comparable structural features and stratigraphic sequences, which allows direct comparison between datasets.

3. Examples of submarine fold-thrust belts

3.1. Gravity-driven fold-thrust belts

3.1.1. Orange Basin, offshore Namibia

The Orange Basin is located on the volcanic-rifted South Atlantic passive margin, offshore southern Namibia and South Africa (Granado et al., 2009). A large delta system (the Orange River) transports a significant volume of material into the basin, generating 1 major and 1 minor classic gravity-driven fold-thrust belts with extension in the upslope region and contraction in the downslope region with the two connected by underlying

basal detachments that dip gently seaward (1-2°) (Fig. 3). To highlight the characteristics of sedimentation and deformation, we remapped the tectonostratigraphic successions and structural features based on previous interpretations (Granado et al., 2009; Butler and Paton, 2010; Morley et al., 2011; Scarselli et al., 2016).

Four distinct stratigraphic units (numbered with increasing age) separated by three regional (inferred) Late Jurassic to Cenozoic unconformities are interpreted (Fig. 3). Sequence I (Late Jurassic) is deformed by landward-dipping extensional growth faults, seaward-dipping stratigraphic reflectors of volcaniclastic strata and associated graben and half graben, reflecting the crustal extension/syn-rift phase (Granado et al., 2009; Scarselli et al., 2016). Sequence II is a transgressive succession of terrestrial sandstones intercalated with basaltic lava and overlain by marine sediments (Gerrard and Smith, 1982; Wickens and McLachlan, 1990; Light et al., 1993; Séranne and Anka, 2005; Mello et al., 2011; Scarselli et al., 2016). The late Lower Cretaceous sequence III and Cenozoic sequence IV are composed of marine post-rift deposits. Sequence III shows more complicated tectono-stratigraphic evolution with flat-lying strata overlain by prograding clinoforms in association with widespread regional growth listric faulting (up-slope) and thrusting and folding (downslope). Overlying Sequence IV is characterised by prograding clinoforms and slope failures.

We differentiate fault types in the interpretation as follows: normal faults are blue, basinward/seaward-verging thrust faults are red, landward-verging thrust faults are black, detachment fault(s) are pink. For poorly resolved fault geometries, a dashed line is used.

In sequence III, the area affected by gravitational deformation can be sub-divided into two systems, a landward/upslope major system (1), and a seaward/downslope minor system (2) (Fig. 3). The minor system (2) forms in the frontal deep sequence below the compressional system associated with (1). It has an overall width of 88 km from extension to contraction, and deforms a very thin pile of material (0.3s two-way time) and is therefore unlikely to have a significant effect on the entire deformational system (i.e. 360 km long and ~3 s thick). For the major gravity-driven system (1), the extensional domain is linked downslope to a contractional domain via a structurally complex and poorly imaged transition zone of ~4 km width (Fig. 3, Table 1). The extensional domain is ~133 km wide and the contractional zone is narrower, ~84 km wide (Fig. 3, Table 1). The extensional domain includes predominantly SW-dipping listric normal faults with fault spacing of 3-10

km. The contractional domain includes SW-directed imbricate thrust sheets with more narrowly spaced thrust faults (~3 km). All thrust sheets terminate in asymmetric SW/seaward-verging fault related folds, interpreted in 2D as fault-propagation folds. Most faults within the extensional and contractional domains are detached onto a common detachment which is interpreted to be controlled by overpressured shale (Scarselli et al., 2016). Due to unresolved stratigraphic detail within Sequence III, we are not able to quantify the deformation characteristics of the normal growth faulting and thrust sequences and hence quantify deformation across the whole system. But clearly some normal faults propagate upwards into Sequence IV, while the thrust faults are limited to Sequence III. Both fault systems are buried without surface expression and are likely not presently active or only slightly active. The majority of deformation takes place during deposition of Sequence III (Aptian-Maastrichtian). The shortening rate across this contractional domain is estimated as 2.3-3.6 mm/yr (Cruciani et al., 2017).

3.1.2. Para-Maranhao Basin, offshore Brazil

The Para-Maranhao basin is located on the South American continental margin, offshore Brazil. An FTB is formed as the downslope expression of large-scale gravitational failure upslope (Fig. 4; Butler and Paton, 2010). The overall gravity-driven deformational system is 38 km wide, composed of a 19 km wide extension region and 16 km wide contraction region that are underlain by a gently seaward dipping detachment and overpressured mudstone (Fig. 4; Butler and Paton, 2010). Seven tectonostratigraphic sequences and associated structural features are interpreted: basement, Pre-kinematic, Growth I, II, III, IV and Post-kinematic (from deep to shallow levels). Each growth sequence represents a discrete stage of fault/fold growth. In cross-section, the majority of sediments are syn-kinematic sequences that attain thicknesses up to ~3 km in the graben basins related to extensional faulting, while a relatively thin pile of sediments (<1 km) is deposited as pre-kinematic sequences. The stratigraphic thickening in this gravity-driven system is attained mainly by deposition, rather than strain through shortening and thrust repetition in the plate convergence-driven system.

To better explain the growth history of extensional faults in relation to deformation initiation and development (migration and localization), we number all the interpreted normal faults in order of timing of initiation based on analysis of the growth stratigraphy. Fault F1 is the primary listric extensional fault with a cumulative displacement of ~14.7

km measured as the offset of the top of the Pre-kinematic sequence, and it dominates strain accommodation in the extensional domain. It is initially induced by the deposition of Growth sequence I as gravity failure, and its subsequent growth created a prominent half-graben basin filled with Growth sequences II-IV. The overlying Post-kinematic sequence marks the cessation of fault F1 growth (Fig. 4). During the continuous growth of F1, accommodating the majority of strain during Growth sequences I-IV, a component of strain is distributed elsewhere within the extensional zone. The first phase of strain migration leads to the formation of normal faults F2 and F3, 8-10 km basinward of F1 (Fig. 4), which deform Growth sequence I and part of Growth II. A second phase of strain migration occurs landward as two normal faults F4 and F5 initiate 2 km into the hanging wall of F1. These faults initiate within Growth sequence II, and continue through Growth sequences III and into IV.

In the contractional domain, all thrust faults are seaward/basinward verging and appear to initiate and grow synchronously, with initial activity coincident with significant growth of major normal fault F1 as documented by Growth sequence I (Fig. 4). Later thrust and associated folding activity is more localized in the rear of the contractional domain, as documented by the thinning and deformation of Growth sequences II, III and IV. The deposition of post-kinematic material marks the cessation of the entire system, with onlap onto developed topography observed within this sequence particularly in the landward part of the contractional domain (Fig. 4).

These results highlight the characteristics of self-powered deformation within a gravity-driven system. The extension of normal faults in the upslope/landward slope region supplies the driving force and energy source to drive thrusting and folding downslope. Once the driving force ceases, the compressional deformation stops.

To estimate the magnitude of deformation, three stratigraphic horizons are used to carry out area balancing analysis and strain measurement, i.e. the tops of the Pre-kinematic (Horizon 1), Growth I (Horizon 2), and Growth II (Horizon 3) sequences (Figs. 4&5). The regional slope is estimated based primarily on the present-day bathymetry (i.e. top of Post-kinematic) that is formed when the system is inactive and therefore is a good approximation for the initial sedimentary slope prior to deformation. For each layer, the area encompassed by the regional slope, faults and selected layer is quantified to evaluate the magnitude of extension and contraction.

The area balancing of Horizon 1 shows that the extension is directly connected with contraction without an obvious temporal transition in this system (Fig. 5a), in contrast to the Orange basin, offshore Namibia discussed above (Fig. 3). Regarding width, the extensional domain extends 21 km basinward whereas the contractional domain is only 13 km wide. By the time of Horizon 2, the extensional domain has propagated only 0.3 km basinward while the contractional domain propagated 1 km basinward (Fig. 5a). By Horizon 3, the extensional domain has retreated slightly, 0.8 km landward, while the contractional domain has propagated landward significantly, ~9.3 km. The measured 8.1-14 km^2 extensional area from the three horizons is much larger than that of the contractional area, 2.8-9.5 km^2. This difference is attributed to layer-parallel shortening, lateral compaction, and ductile deformation (Sans et al., 2003; Koyi et al., 2004; Butler and Paton, 2010; Şengör and Bozkurt, 2013; Lathrop and Burberry, 2017). The strain across the extensional and contractional domains is also measured as the difference between restored and current bed length for each selected horizon (Fig. 5c). The results show that strain in the extensional domain (4.2-14.4 km, relative to each horizon) is much larger than for the contractional domain (0.2-4.2 km). This is in agreement with the area balancing analysis across the two domains (Fig. 5b). As expected, strain is greatest for the deepest horizon and shows a general pattern of decreasing upwards (Fig. 5a). It is estimated that the shortening rate of this contractional domain is as low as 0.8 mm/yr (Cruciani et al., 2017).

We note this seismic section is mapped (Butler and Paton, 2010) primarily based on its tectonic history without emphasis on stratigraphy. The top of the Pre-kinematic sequence for thrusting may in fact be diachronous, with the thrust faults developing in a piggyback sequence, rather than synchronously. However, the continuous growth of the thrusts at the rear of the contractional domain is evident (Fig. 4), and this continues until the extensional faulting stops.

3.1.3. Amazon fan, offshore Brazil

The submarine Amazon Fan lies off the NE coast of Brazil, near the mouth of the Amazon River. It is characterised by a wedge of clastic sediment up to 10 km thick deposited since 10 Ma (Cobbold et al., 2004) (Fig. 6a). Extensional faults have formed across the prograding delta slope and contractional folds and faults have formed seaward of it. The two domains are underlain by a concave detachment above overpressured shale that dips

gently seaward upslope and dips gently landward downslope. In the present-day, the system is composed of a 131 km wide extensional domain and 90 km wide contractional domain, separated by a 11 km wide transition zone of minor deformation beneath the rear of the downslope region (Fig. 6a, Table 1).

An interpreted 2D seismic profile across this system is analysed here, with five tectono-stratigraphic horizons and sequences mapped previously from deep to shallow levels (Fig. 6a; Cobbold et al., 2004; Morley et al., 2011). In this example, Basement is defined as the sequence purely deformed by syn-rift extension (as indicated by deeper normal faulting), pre-dating the gravity-driven system. The top of this unit is marked by the Top Cenomanian. The rifting-related extension terminates between the top Cenomanian and top Cretaceous and this unit (medium green colour) is partly syn-rift and partly post-rift (Fig. 6a). The Pre-kinematic sediments (light green) thin basinward. This would produce a prominent topographic relief/slope with the resulting gravitational energy enabling the system to deform. The stratigraphic thickening in this system is attained mainly by deposition as represented by the up to 7 km thick Growth sequence I-II.

In terms of structural styles, the normal faults are predominantly regional, dipping basinward with a few outliers of counter-regional normal faults dipping landward, however the thrust faults are typically basin/seaward-vergent. The detachment is developed between the Top Cenomanian and Top Cretaceous in the extensional domain and the landward region of the contractional domain (medium green), but coincides with the Top Cretaceous for the more seaward part of the contractional domain based on previous interpretations (Morley et al., 2011). The majority of normal and thrust faults detach onto this level.

Regarding growth/activity history, the linked system starts to deform at the time of Top Cretaceous deposition, and continues until the present-day with some normal faults extending to the seafloor and the thrust faults dying out beneath the seafloor. Although blind (interpreted as a result of low uplift and high sedimentation rates (Shaw et al., 2005), activity of the thrust faults in the most recent depositional phase is supported by thinning of the Growth II succession above the Top Pliocene towards the anticlinal crests (Fig. a). Extensional and contractional strain across the system have been quantified using three sedimentary layers separated by the following horizons: (Horizon 1) Top Cretaceous, (Horizon 2) base Amazon Fan, and (Horizon 3) Top Pliocene, using the same method as

described for the Para-Maranhao basin above. The results show a strain difference and pattern between the extensional and contractional domains (Fig. b). This can be generally explained by lateral compaction, commonly recognized in poorly lithified sedimentary successions, e.g. the Orange basin offshore Namibia (Butler and Paton, 2010). We note that the strain difference between extension (17.6 km) and contraction (1.9 km) from the deepest horizon (Horizon 1, Top Cretaceous) is very large with respect to the other horizons, i.e. 6.4-9.1 times (Fig. b). However, this anomaly is interpreted to result from errors in interpretation. For example, there are only 1-2 thrust faults interpreted relative to 11 normal faults, which is obviously unbalanced in such a large gravity-driven system (Fig. b). Therefore, we suggest that the Top Cretaceous should be above the basal detachment across the contractional domain, rather than beneath it. In addition, the correlation of horizons and stratigraphic units between the extensional and contractional domains may not be completely accurate. The shortening rate across the contractional domain is estimated at as low as 0.9-1.4 mm/yr (Cruciani et al., 2017).

3.1.4. Niger delta, offshore Nigeria

The Niger Delta, on the West African continental margin, has a well-developed large delta province with an onshore to shelfal zone of growth fault-controlled depocentres, a belt of shale diapirs around the outer shelf-slope area, and a fold-thrust belt in the slope area (e.g. Evamy et al., 1978; Doust and Omatsola, 1989; Morley and Guerin, 1996; Haack et al., 2000; Ajakaiye and Bally, 2002) (Fig. 7). The extensional domain is 93 km wide and contractional domain 89 km wide, separated by a 41 km-wide transition zone of minor deformation (Table 1). The basal detachment dips gently seaward beneath the extensional domain and landward beneath the contractional domain (Fig. 7), and has been interpreted as within or at the top of overpressured, compacted shale (Bilotti and Shaw, 2005; Higgins et al., 2009; Morley et al., 2011; King and Morley, 2017).

The interpreted seismic profile across the Niger delta, Gulf of Guinea, used here consists of four principal tectono-stratigraphic sequences: Basement, Cretaceous, Pre-kinematic and Syn-kinematic (Fig. 7). The Basement is the oceanic crust subjected to extension during the crustal stretching/syn-rift phase. The overlying post-rift sequence is deposited during the Cretaceous ("Cretaceous" sequence) and the Pre-kinematic sequence is deposited during the Paleocene to Miocene. Similar to the observation made in the Para-Maranhao basin (Fig. 4) and Amazon fan (Fig. 6), the thickened region (extensional

domain) is largely attained by the deposition of a thick syn-kinematic sequence, which in turn powers the system as the source of gravitational potential energy.

In terms of structural style, the extensional domain is characterised by both regional and counter-regional listric and planar normal faults while the contractional domain is made up of a range of seaward-verging thrust faults that tip out upwards without distinct seafloor expressions and are not back rotated.

Deformation in the extensional domain is dominated by two major listric normal faults (one regional, one counter-regional) with a component of deformation accommodated by a number of minor, rootless normal faults, while in the contractional domain deformation is accommodated by a number of imbricate thrusts, rather than individual major structures. The initiation of extension is marked by the major counter-regional listric fault in the extension domain where the thickened syn-kinematic sequence is developed. Subsequently, deformation propagates mainly basinward with a minor component of landward propagation. The initiation and continuation of shortening coincides with the growth of new normal faults (Fig. 7). In the present day, the major contractional deformation appears to occur in the middle of the contractional domain where fold growth significantly deforms the seafloor relative to surrounding areas (Fig. 7a). We note the seismic section used here probably does not include the entire seaward part of the contractional domain. A maximum shortening of 17-25 km is estimated across the contractional domain (Corredor et al., 2005; Table 1) across which the shortening rate is estimated as 1.4-2.0 mm/yr (Cruciani et al., 2017).

Wu and McClay (2011) reported that in this system the sequence of thrusting tends to young offshore, and most folds and thrusts verge basinward, typical for a critical wedge model. However, studies from an adjacent area report examples of out-of-sequence thrusting, synchronous deformation and break-back sequences, with some folds displaying pop-up and triangle-zone geometries, and a series of back-thrusts (e.g. Morley, 2003; Corredor et al., 2005). Therefore there are clear variations in structural style along strike and the contractional domain is unlikely to be a simple piggyback thrust sequence throughout.

Journal Pre-proof

3.2. Plate convergence driven fold-thrust belts

3.2.1. Nankai accretionary prism, offshore Japan

The accretionary Nankai subduction margin forms where the Philippine Sea Plate converges and subducts beneath SW Japan and Eurasia, which is a regular site of large earthquakes. It is a typical plate convergence-driven FTB end member. A cross section across the prism (Muroto transect) shows the characteristics of fold and fault geometry and the associated sedimentary sequence across a width of 21 km (Fig. 8). Building upon previous work (e.g. Moore and Silver, 1987; Moore et al., 1990; Hills et al., 2001; Bangs et al., 2004; Gulick et al., 2004; Wu and McClay, 2011), we mapped faults and four key tectono-stratigraphic sequences: Basement, Miocene, Pre-kinematic and Syn-kinematic (Fig. 8). The basement here is oceanic crust of the subducting plate, while the Miocene sediments are the subducted sedimentary materials overlying basement.

Bangs et al. (2004) mapped the subduction thrust reflector from the trench into the seismogenic zone using 3D seismic data supported by drilling data, and showed that the décollement forms within the lithologically homogeneous Lower Shikoku Basin facies along a high-amplitude reflection, potentially high pore fluid pressure. It is a major boundary for both physical and mechanical properties (Moore et al., 2001) between the underthrusting Miocene sequence and Pliocene-early Quaternary pre-kinematic sequence, and dips 6-8 ° landward (Fig. 8). .

The deforming sediments (Pre-kinematic), attaining thicknesses up to 3 km, are input and continuously supplied by the subducting oceanic plate. The syn-kinematic sediments experience only minor deformation and are thin (< 0.3 km), in contrast to the pre-kinematic sequence which is significantly deformed and relatively thick (up to 2 km). This shows that the thickening of plate convergence-driven FTBs is attained by shortening and thrust repetition and not the build-up of syn-kinematic sediment thickness, in contrast to the thickening being produced by deposition of the deformed syn-kinematic sequence within gravity-driven FTBs.

The Nankai fold-thrust belt is a well ordered array of closely spaced (1–2 km) basinward-vergent thrusts with associated folds. Several of these thrusts, primarily further landward, have developed landward-verging backthrusts in the shallow part of the section (<1 km beneath seafloor) (Fig. 8). The majority of the discrete thrusts separate the fold-and-

thrust sequences of the accretionary wedge and sole out into the basal detachment (Fig. 8, see also Bangs et al., 2004). Unlike the thrusts of a gravity-driven FTB largely buried by a thick syn-kinematic sequence, there is a distinct seafloor expression of thrust faults and associated folds in this system, i.e. most/many of the thrust faults are not blind.

In terms of deformation history, the syn-kinematic succession is time transgressive, and the thrusting sequence is therefore not synchronous, but likely younging basinward (e.g. Moore et al., 1990; Moore et al., 2001; Moore and Saffer, 2001). The overall convergence rate across the Nankai accretionary prism is estimated as ~40–60 mm/yr using GPS measurements (Seno et al., 1993; DeMets et al., 2010; Loveless and Meade, 2010).

3.2.2. Hikurangi accretionary prism, offshore New Zealand

The Hikurangi accretionary prism is located above the subducting oceanic Pacific Plate on the eastern margin of the North Island, New Zealand (Barnes et al., 1998; Barnes et al., 2010). It is a typical plate convergence-driven FTB. In the example profile from the central Hikurangi margin (Fig. 9), an ~90 km wide prism is interpreted with seven stratigraphic horizons of inferred age 30+/-5 Ma to present by previous authors (Ghisetti et al., 2016). Here we reinterpret the sequence to highlight its tectonic history while maintaining the previously interpreted stratigraphic horizons. This allows direct comparison of structural initiation development with sediment deposition.

The sedimentary material within the thrust belt is dominated by the up to 6 km thick Pre-kinematic sequence, with three thin (up to 1 km thick) Growth successions (I-III) deposited at shallow depths, <1 km beneath the seafloor (Fig. 9). This prominent contrast in sediment thickness is similar to that observed in the Nankai accretionary prism (Fig. 8), with thrust repetition and folding, not deposition, dominating section thickening.

The structures in this cross section are dominated by basinward/seaward-verging imbricate thrust faults and associated fault-propagation folds. Minor faults are observed splaying off the shallow portion of a few major thrust faults, and 4-5 rootless backthrusts are observed in the hanging wall of some of the major imbricate thrusts. Some major thrusts show listric geometry with an increasing fault dip upward (Fig. 9, note these are depth sections so this is not a velocity effect on fault dip).

In terms of growth history, the Growth I sequence is deposited during the development of the early thrusts now at the rear of the wedge. The overlying Growth II sequence extends

10 km further basinward relative to Growth I, indicating the forward propagation of the wedge with formation of additional thrusts. Growth III is deposited beyond the previously developed thrust faults, and extends to the deformation front across the majority of the fold belt (~35km wide). The wedge deformation is therefore characterised by forward propagation involving sequential (Growth I and II) and synchronous (Growth III) development of thrust faults.

Ghisetti et al. (2016) estimated a total of 16.6 km shortening accommodated by thrusting and folding since the deposition of Horizon R5 (2.0+/-0.8 Ma, Fig. 9) by using sequential restoration. The present-day convergence rate is estimated as 43-48 mm/yr (DeMets et al., 1994; Walcott, 1998; Beavan et al., 2002; Wallace et al., 2009).

3.3. Combined gravity- and plate convergence-driven fold-thrust belts

Unlike the end member scenarios driven entirely by gravity, such as the Niger Delta, or plate convergence, such as the Nankai margin, a hybrid system of fold-thrust belt with components of both drivers might be expected to inherit the structural characteristics of both types of system. The Makran is a subduction zone with a gravitational element at least in part of the along-strike system (observed on part of the Iranian margin, e.g. Grando and McClay, 2007) and the NW Borneo margin of Brunei is a gravity system with a possible subduction/convergence element (Hesse et al., 2009; King et al., 2010a).

3.3.1. Makran accretionary prism, offshore Iran

Of global subduction zones, the Makran has the largest documented input sediment section, as a result of Indus Fan subduction, and the widest accretionary wedge system (~350 km, e.g. Smith et al., 2012). It is formed as a result of subduction of the Arabian plate beneath the Eurasian plate throughout the Cenozoic (Harms et al., 1984b) offshore Pakistan and Iran. In the west, offshore Iran, a regional N-S geological cross-section (Fig. 10) shows that the margin is also deformed by a 47 km wide extensional domain on the shelf in the form of growth normal faults, and an 85 km wide compressional domain further downslope forming the seaward part of the accretionary prism (Grando and McClay, 2007). The two deformation zones are underlain by a gently north-dipping, sub-horizontal basal detachment (Fig. 10a&b).

Building on previous interpretations (e.g. Grando and McClay, 2007), six stratigraphic

units are mapped from deep to shallow levels on one seismic profile (Fig. 10a): Himalayan Turbidites, Makran Sands, Growth II, Growth III, Growth IV and Chaotic zone. The cross section is then structurally reinterpreted to highlight its deformation history (Fig. 10b). Three types of deformation-related sedimentary successions are mapped: (1) Basement, (2) Pre- kinematic, and (3) Growth (broken into units I-IV), i.e., the sediments deposited during deformation. Note Growth sequence I in Figure 10a defined by Grando and McClay (2007) is broken into Growth sequence I and II in Figure 10b, with the first one corresponding to extension and the second one corresponding to compression. The chaotic zone could represent shale diapirs, narrow shale pipes or gas chimneys (Morley et al., 2011).

The primary listric normal fault (northern end of profile) and all basinward-/seaward-verging thrust faults detach onto this level (Fig. 10b), whereas the more minor normal faults (between faults F1 and F2) and the two minor landward-verging thrust faults (or backthrusts) in the contractional domain appear to be rootless, dying out at depth with negligible displacement. These rootless faults are interpreted as secondary structures and have very limited effect on the overall development of Makran accretionary prism.

In this evolving thrust system, Growth sequence I represents the first stage of deformation, and is thickest in the extensional domain, including in the half-graben basin created by the major extensional fault F1, with a thinner section preserved in the hanging walls of thrust faults F2 and F3 (Fig. 10b). The distribution of Growth I indicates the coincidence of activity of extensional and thrust faults in this coupled system. This first-stage deformation extends as far as thrust fault F3 but not beyond, and involves the landward part of the Makran Sands sequence (Fig. 10a). Subsequently, three stages of deformation are recognized, denoted Growth II, III and IV and these phases appear to involve the entire extensional to contractional system (they are widely distributed) and mark a change in activity and extent of the system between Growth I and II.

The thicknesses of Growth units II, III IV change within the hanging walls of the thrust faults (primarily thinning towards the crest), but have more constant thickness across the normal fault hanging walls, in particular near the primary listric normal fault, F1 (Fig. 10b). This suggests that major deformation is focused in the contractional (FTB) domain with minor deformation in the extensional domain since Growth II. Therefore, gravitational failure may have only played a role in driving thrust faults F2 and F3 (Fig. 10b), with

subsequent contractional deformation driven primarily by plate convergence. However, it is possible that additional normal faults exist upslope (Harms et al., 1984a; Hosseini-Barzi and Talbot, 2003; Burg et al., 2013; Burg, 2018) (beyond the northern end of the seismic profile) with larger displacements and extension, playing a bigger role in generation of the thick Growth sequences in the extensional domain (in particular Growth I, Fig. 10b).

To validate this observation and the significance of gravity-driven extension, we further quantify the magnitude of deformation across the extensional and contractional domains. Because this is a time section, we choose to measure fault heave as a proxy for strain and relative strain distribution. Four stratigraphic horizons are used to carry out the strain measurement: top of Himalayan Turbidites (Horizon 1), top of Makran Sands (Horizon 2), top of Growth II (Horizon 3), and top of Growth III (Horizon 4) (Fig. 10a). The results show fault heave not surprisingly decreases updip from the deepest (1) to shallowest horizon (4) for both the extensional and contractional domains. We note that heave relative to displacement changes with depth for listric faults, particularly affecting the normal faults here, and therefore will artificially exaggerate a decreasing upward heave. The heave of the extensional faults amounts to 3.3, 1.2 and 0.6 km for Horizons 1,2 and 3, respectively, which is 11.4%, 6.8% and 8.1 % of the 33.2, 17.8 and 7.5 km heave of the thrust faults for corresponding horizons, demonstrating the dominance of thrusting over normal faulting in accommodating strain in this system (Fig. 11). The total heave in both deformational domains reduces upwards as the lowest value is documented by Horizon 4 (the shallowest horizon), i.e. 0.4-0.5 km. This is interpreted as the effect of updip propagation of deformation and the buried nature of the thrust faults. Horizon 4 in the contractional domain is the top of Growth III (Fig. 10a), which is largely affected by folding, and not by fault displacement. Because this study only quantifies fault heave rather than fold shortening as a component of deformation (Fig. 1), the overall deformation is underestimated and in particular for Horizon 4.

In the present-day, the average convergence rate is ~40 mm/yr approximately northward, varying from 36 mm/yr in the west to 42 mm/yr in the east (DeMets et al., 1990). More recently Vernant et al. (2004), based on GPS data, have estimated convergence velocities of 27 mm/yr in the western Makran.

We conclude that the Makran accretionary prism is predominantly a plate convergence-driven system (Growth II- IV) with minor gravitational contribution primarily in the first

growth stage (Growth I), however evidence for additional deep reaching extensional faulting beyond the profile used would increase this component.

3.3.2. NW Borneo deepwater fold-thrust belt, offshore Brunei

The NW Borneo deepwater fold-thrust belt is interpreted to result from a combination of gravitational instabilities and active regional collision (e.g. Ingram et al., 2004; Morley, 2007; Hesse et al., 2009; Hesse et al., 2010; King et al., 2010a). The system is composed of two deformational domains: upslope extension (46 km wide) and downslope contraction (85 km wide), connected by a common underlying detachment interpreted as preferentially located at weak over-pressured mudstone (e.g. Van Rensbergen and Morley, 2003; Ingram et al., 2004; Morley, 2007) (Fig. 12b). The first-order geometry of the detachment is a ramp-flat-ramp, excluding the estimated landward trace (dashed line, Fig. 12a). Similar to the Makran prism (Fig. 10a), there is no observed transition zone between the two deformational domains.

Four major, counter-regional normal faults and the majority of seaward-verging thrust faults appear to sole out into the basal detachment (Fig. 12a). The remaining normal faults are regional (i.e. seaward dipping), and either die out at depth or intersect with another fault, while the remaining thrust faults are up to 2 km above the detachment, characterized by decreasing displacement updip (Fig. 12a).

Six tectonostratigraphic units are mapped from previous interpretations (Morley et al., 2011; Morley et al., 2014): Middle Miocene and Older, Middle Miocene, Upper Miocene, Upper Miocene-Pliocene, Pliocene and Pleistocene-Holocene (Stratigraphic notation of Morley et al. (2014); Fig. 12a). To reinterpret tectonic history, we mapped eight tectonic-related sequences: Basement, Pre-kinematic, Growth I, II, III, and IV, and Post-kinematic (Fig. 12b).

The first stage of deformation (Growth I) initiates in the extensional domain where the maximum cumulative displacement is accommodated by two conjugate normal faults, F1 and F2, forming a graben. Deformation then propagates predominantly basinward with minor landward propagation, and is characterised by decreasing fault displacement as documented by Growth II. This second stage of deformation (Growth II) involves the majority of the normal faults and two thrust faults at the rear of the contractional domain (Fig. 12b). During this stage, most normal faults (including all basinward-dipping faults)

become inactive with fault dying out upwards within Growth II, but three landward-dipping normal faults remain active. Deformation during this stage propagates ~10-12 km basinward due to the formation of the two new thrusts (F3 and F4). The third stage of deformation (Growth III) is characterised by continuous activity on three primary landward-dipping normal faults and 3-4 newly activated thrust faults seaward of F3 and F4. This stage involves an additional 15 km of basinward propagation of deformation. The fourth stage (Growth IV) marks the cessation of growth of the three landward-dipping normal faults and formation of one new thrust fault, ~20 km basinward. The fifth (final) stage of deformation (Growth V and Post-kinematic) is more complex, with all normal faults inactive but the majority of thrusts beyond F4 active (Fig. 12b). If this cross-section includes all extensional structures across the margin, then this final stage of thrusting (Pleistocene-Holocene) must have been driven by regional active collision with an absence of gravitationally-driven deformation. This agrees with small but not insignificant present-day convergence between NW Borneo and Sundaland of 4-6 mm/yr (Simons et al., 2007; Sapin et al., 2011; Sapin et al., 2013) and greater downslope shortening than upslope extension estimated from sequential restoration of Hesse et al. (2009) (King et al., 2010a).

To highlight the deformation history, we created a schematic of the five stratigraphic units broken down into the tectonostratigraphic units for extension and contraction (Fig. 12c). The width of each unit correlates to the interpreted seismic section above, which shows the position and extent of deformation at each stage. The map indicates that extension initiates in the Middle Miocene, and then propagates mainly upwards with only minor forward propagation (E in Fig. 12c), and ceases during or just before the Pleistocene-Holocene (P in Fig. 12c). In contrast, contraction initiates later, during deposition of the Upper Miocene. Subsequently, it propagates forwards significantly as highlighted by the basinward/seaward extent of contraction (C in Fig. 12c). In the Pleistocene-Holocene, the rear of the contractional domain, in the form of early formed thrusts and folds, is inactive (P in Fig. 12c) but there is continuous deformation of a wide zone of thrust and folds in the outer part of the FTB (C in Fig. 12c).

Our structural analysis indicates that, in general, the NW Borneo fold-thrust belt is predominantly a gravity-driven system with a minor contribution from plate-scale

shortening produced by far-field plate-convergence, in particular during the recent Pleistocene-Holocene stage.

4. Discussion

4.1 Driving forces and energy source

The energy source of gravity-driven systems is the release of gravitational potential energy (PE) within the linked system (Peel, 2014). For large-scale passive margin systems, this is energy contained within the sediment pile itself, i.e. within the body of material that is being deformed (the deformed syn-kinematic sequences in the hanging wall of upslope extensional faults in Figs. 3,4,6,7), and the energy is supplied to the linked system through the means of body forces that are applied to the moving sediments. The system is contained within outer boundaries that do not need to move. Natural gravity-driven systems generally require the existence of a height differential between the ends of the system, usually in the form of a surface slope, e.g. the estimated surface slope in the Para-Maranhao basin, offshore Brazil (Fig. 4). The greater the height difference, the greater the PE and potential for development of a gravity-driven system. This height difference can change through time dependent on the rate of addition of sediments or as the slope system deforms and sediments are incorporated. It is worth noting that the gravitational PE driving lateral motion could also exist in a system without any initial surface height difference, if sediment density changes laterally. But there is no such known major example.

In contrast, the energy source of plate-convergence driven systems is the movement of the stressed lithospheric-scale boundary, which lies essentially outside the local sediment pile. It is supplied to the FTB through the means of boundary forces (relative plate motions) applied to a moving boundary. The FTB system is contained within outer boundaries that must move.

As a consequence, the sediments in gravity-driven FTBs are dominated by significantly deformed syn-kinematic sequences, typically >3 km in thickness, that power the system in the form of PE, particularly in the extensional domain, but with much thinner (<1 km) pre-kinematic sequences (Figs. 3,4,6,7). In contrast, plate convergence-driven FTBs are typified by thick pre-kinematic sequences (2-7 km) with very thin (<0.5 km) and slightly deformed syn-kinematic sequences across the system (Figs. 8&9). We conclude that the

sequence thickening is generated by deposition of the syn-kinematic sequence in the gravity-driven system but by shortening and thrust repetition in the plate convergence-driven system (Table 2).

4.2 Resupply and renewal of energy, and the link to deposition

In order for a system to continue for long periods of time, and to accumulate large lateral displacements, the energy supply needs to be recharged. Gravity-driven systems can arise on slopes without energy resupply, but as they move, they use up the energy, and so will slow down and ultimately stop. Furthermore, by Le Chatelier's Principle, movement of any dynamic system that is close to equilibrium tends to change the system in such a way as to oppose movement. For example, in a gravity-driven linked system, movement of material deepens the upslope extensional area and shallows the downslope contractional area (Fig. 4), thus decreasing the overall slope (Rowan et al., 2004). Energy recharge within gravity-driven systems can be any process that adds new (sedimentary) material which has PE by virtue of its position, or any process which increases the PE of the existing material. In natural gravity-driven systems, this recharge most commonly occurs by addition of new sediment in the updip part of the slope, such as observed thick syn-kinematic deposits in the half graben basins created by extensional fault growth (e.g. Figs. 4,6,7). Tectonic uplift of the updip part of the system (e.g. by basement faulting or regional tilting) can also increase the PE of the system, e.g. the gravitational potential energy between the uplifting mountains and lowlands in New Guinea, Southern New Zealand and Himalaya-Tibet (Copley et al., 2009; Copley et al., 2011).

Consequently, there is a common genetic linkage between the development of large scale gravity-driven systems and major sediment input. The major gravity-driven systems tend to be linked to major sedimentary systems in particular river deltas (e.g., Niger, Mississippi, Orange rivers), and the timing of major episodes of movement are probably linked to major episodes of sediment input. Rates and magnitude of sedimentation are primarily functions of climate change (e.g. Burbank et al., 1996; Whipple et al., 1999; Hales and Roering, 2005; Riebe et al., 2015), therefore deformation in gravity-driven linked systems are likely controlled indirectly or directly by climate variation. Future research efforts combining structural geology, sedimentation and paleoclimate are required to confirm this hypothesis.

Journal Pre-proof

In a system driven by plate convergence, the energy enters the system by movement of a boundary upon which a force is acting. The energy is consumed by deformation, by processes such as the raising up of sedimentary material within the orogenic wedge (e.g. Chapple, 1978; Davis et al., 1983). The energy is resupplied by ongoing plate convergence and further movement of the boundary. This will occur regardless of whether there is major sediment input, or whether the margin is sediment starved and purely reliant on maintenance of the convergence between the plates. The addition of sediment to such a system (i.e., the syn-kinematic sequence) will modify the response of the system, and change its structural style. For instance, previous studies indicate that high syn-tectonic sedimentation widens a plate convergence-driven FTB, reduces the number of imbricate thrusts and taper angle, and inhibits fault activity (Storti and McClay, 1995; Wu and McClay, 2011; Buiter, 2012; Fillon et al., 2012; Wang et al., 2013). The addition of sediment seaward of the deformation front supplies the sediment to be accreted, thrusted and folded in the form of the pre-kinematic sequence (e.g. Fig. 10). But it is not a necessary component to power the system which is demonstrated by the significant deformation in the Nankai, and Hikurangi accretionary prisms, but very thin (<0.5 km) syn-kinematic sequence (Figs. 8&9). The thickness of the incoming sedimentary section at a subduction zone does however have a major control on the scale and extent of the FTB. The largest sedimentary sections exist where submarine fan systems are being accreted, e.g. Indus (Makran), Bengal-Nicobar (Sunda/Sumatra-Myanmar), and width and thickness of the FTB is clearly linked to thickness of the input sequence (e.g. Smith et al., 2012; McNeill and Henstock, 2014).

4.3. Structural styles

4.3.1. Normal faults

In the gravity-driven system, listric normal faults tend to dominate, often soling out deeply into the primary detachment, whereas planar normal faults are in the minority and are often rootless, dying out above the detachment (Figs. 3&10). In terms of fault-dip direction, regional, seaward-dipping normal faults dominate over landward-dipping normal faults in the extensional domain. Regarding strain localization, the listric normal faults dominate strain accommodation relative to planar normal faults, as demonstrated by the significant displacement of listric normal faults (up to 14 km) and negligible

displacement (<0.3 km) of planar normal faults in the Orange basin, Para-Maranhao Basin, Amazon Fan and Niger delta (Figs. 3,4,6,7).

This observation is also applicable to the hybrid deformational system examples presented here (NW Borneo and Makran). For NW Borneo, gravitational failure is interpreted as dominant whereas for the Makran, gravitational failure is interpreted as a minor driver of fold-thrust belt development. For the purely plate-convergence driven (accretionary) systems examined here (Nankai, Hikurangi) and elsewhere, there is no evidence for major normal faulting, although minor shallow extension is sometimes associated with anticlinal crestal flexure or collapse. We note however that erosional convergent margins, often controlled by subducting basement topography, commonly include significant extensional fault systems and associated subsidence (e.g. Costa Rica, Ranero and von Huene (2000)).

4.3.2. Thrust faults and related folds and detachment properties

The thrust faults in the contractional domain of the fold-thrust belts in this study are predominantly seaward-verging imbricate thrusts detaching onto a basal detachment (Figs. 3&10). Several major thrust faults in the Hikurangi accretionary prism are not detached (Fig. 9), but this may be a function of seismic resolution, i.e. unresolved structures at depth. Backthrusts are only observed in the purely or predominantly plate-convergence driven systems, such as Nankai, Hikurangi and Makran (Figs. 8,9,10). These faults typically arise in the hanging wall of imbricate thrusts as secondary conjugate structures with minor displacement, although they can be the primary thrusts (e.g., parts of the Cascadia, Sunda margins, MacKay et al. (1992). Back rotation of thrusts is also only observed at the rear of the plate convergence-driven or dominated system such as Nankai, Hikurangi and Makran (Figs. 8,9,10, Table 2). Both backthrusts and back rotation are absent from the purely or predominantly gravity-driven systems (Table 1, Table 2).

Rowan et al. (2004) suggest the fold structural style in FTBs is independent of the driving mechanism, and is largely dependent on the nature of detachment. However, the folds in these systems, many of which may be controlled by overpressured shale and mudstone, are dominated by fault-propagation folds (Figs. 3&12, Table 1). This contradicts the statement of Rowan et al. (2004) that symmetric, low-relief detachment folds most commonly arise above a weak basal detachment, i.e. salt, overpressured shale, and

asymmetric and basinward-vergent folds and imbricate thrusts are mostly developed above a strong basal detachment, as also suggested by Davis and Engelder (1985).

In addition, the basal detachment typically dips gently seaward in the gravity-driven system but dips landward/towards the hinterland in the plate convergence-driven system (Table 1, Table 2). The presence of a seaward-dipping surface slope supplies the gravitational potential energy for the gravity-driven system, which leads to the formation of a seaward-dipping basal detachment. In contrast, the plate convergence-driven system is part of a subduction zone where the plate boundary (basal detachment) naturally dips landward.

4.4. Strain distribution

In a gravity-driven system, the upslope extensional strain is larger than the downslope contractional strain and decreases from deep to shallow levels, such as 3.0-14.4 km (extension) vs 0.2-4.2 km (contraction) in the Para-Maranhao basin and 4.8-18.5 km (extension) vs 0.9-14.0 km (contraction) in the Amazon system (Figs. 5&6). We attribute this apparent strain difference to lateral compaction (Butler and Paton, 2010), layer-parallel shortening (Koyi et al., 2004), and sub-seismic deformation (Lohr et al., 2008). In the hybrid Makran system, the much reduced extension (heave only) of 0.5-3.8 km is significantly less than the contraction (heave only) of 0.4-33.2 km (Fig. 11), which demonstrates the dominant driving mechanism of plate convergence on FTB deformation. For the hybrid NW Borneo FTB, data from this study (Brunei) and further north (Sabah, 50-100 km NE of our study area) show a more significant convergence component has been involved. For the Sabah portion, Hesse et al. (2009); Hesse et al. (2010) reported net shortening (0-4 km) relative to extension for the Late Pliocene-Holocene, and for the Brunei portion, King et al. (2010a) reported 2 km net shortening relative to extension for the last 0.5 Ma, attributed to regional plate convergence. This highlights the importance of change over time for many of these systems, particularly those that are gravity dominated.

4.5. Deformation initiation and propagation

In general, a piggyback deformation sequence is observed in each FTB system regardless of driver, where deformation initiates adjacent to the upslope extensional region for a

gravity-driven system, or in the hinterland/rear of the FTB in a plate convergence-driven system, and progressively propagates basinward through time (Figs. 3&12, Table 1). For those systems with a poorly resolved syn-kinematic stage (i.e., where we use one syn-kinematic/growth unit throughout such as the Orange basin, Niger delta and Nankai prism, Figs. 3,7,8), previous studies (e.g. Morley, 2003; Corredor et al., 2005) and this study suggest that the sequence of thrusting tends to young offshore, but there are instances of out-of-sequence thrusting, synchronous deformation or break-back sequences on a number of thrusts and folds.

In the gravity-related system (including the hybrid system), deformation initiates in the extensional domain in the form of normal faulting, followed rapidly by the formation of thrust faults in the contractional domain for prism imaged in this study. For instance, Growth I in the Makran prism, offshore Iran (Fig. 12), and Growth sequence I in the Para-Maranhao basin, offshore Brazil (Fig. 4), represent both the extensional and contractional domains. In the system driven purely by gravitational failure, extensional deformation is controlled by major listric faults soling out deeply into the detachment that continue to grow until the system runs out of energy and ultimately stops (Figs. 3,4,6,7). During this process, a range of minor, short-lived normal faults initiate in and deform the hanging wall basin created by the growing major listric fault, and a portion of deformation migrates to these smaller normal faults (e.g. Para-Maranhao basin, Amazon Fan, Niger Delta, Figs. 4,6,7). There is no consistent direction of propagation of minor deformation within the extensional part of the system; it can be either basinward or landward. In the contractional domain of a gravity-driven system, deformation initiates across a wide zone of thrust faults (e.g. Para-Maranhao basin and Niger delta, Figs. 4&7) that form synchronously with each other and with the initial growth of the major listric fault. The subsequent deformation tends to become localized on a few continuously growing thrust faults either at the rear (e.g. Amazon Fan, Fig. 6) or in the middle of the contractional domain (e.g. Niger Delta, Fig. 7).

In summary, despite observed differences between individual examples, a few characteristics appear to be universal in the gravity-driven system: deformation propagates from extension to contraction but rapidly after extensional deformation initiates; deformation in the extensional domain is typically dominated by one or more major listric faults; deformation in the contractional domain initiates synchronously on

Journal Pre-proof

multiple thrust faults; following initiation, deformation localizes onto a few major structures within each domain with a small portion of deformation then accommodated across smaller and short-lived faults.

These observations made for the purely gravitational system are also applicable to the system driven mainly or partly by gravity, e.g. NW Borneo. The interpreted syn-kinematic sequence allows differentiation of the two driving mechanisms in this example, showing that pre-Pleistocene deformation includes activity on both extensional and contractional structures (driven by gravity) but Pleistocene-Holocene deformation is entirely contractional and extensional faults are inactive, resulting from convergence only. In the Makran prism, early activity of the gravity-driven extensional structures (Growth I sequence, Fig. 10) drive the formation of the earliest thrusts at the rear of the contractional domain, followed by Growth II-IV sequences with extensional inactivity and the primary driver of contraction interpreted as plate convergence, continuing to the present day.

4.6. Rates of movement

The rate of movement in the FTBs driven by plate motion is governed by the absolute and relative motions of the plates. Although there will probably be local and short term variations in the rate of shortening within the system, and longer term plate convergence rates can change, the rate is constant and continuous on a relatively long time scale. In contrast, within a gravity-driven system there is no extrinsic constraint on the rate of movement. Rates of shortening are generally very slow in gravity driven FTBs, such as 1.4-2.0 mm/yr in the Niger delta, 2.3-3.6 mm/yr in the Orange basin and 0.8 mm/yr in the Para-Maranhao basin (Cruciani et al., 2017), whereas rates of convergence are an order of magnitude higher at plate convergent systems, such as 27-42 mm/yr in the Makran (DeMets et al., 1990) and 43-48 mm/yr in Hikurangi (DeMets et al., 1994; Walcott, 1998; Beavan et al., 2002; Wallace et al., 2009) (Table 2). It is also possible for gravity-driven movement to be much faster and even catastrophic and highly variable. This is because sediment flux to the margin via deltaic systems can change significantly in response to regional climate change, surface processes or change in morphological structure of the delta system (e.g., lobe switching).

The entire crust/lithosphere is involved in plate-convergence driven systems, even though the frontal portions (often the entire FTB being examined here) are typically thin-skinned. Moreover, both the total amount of shortening and the deformation rates are usually substantially higher than in gravity-driven FTBs. The rate of convergence across plate-convergence driven FTBs is continuous on a long time scale and very high in magnitude (e.g. 43-48 mm/yr in Hikurangi, 40-60 mm/yr in Nankai), being of orders of magnitude higher than those of the gravity-driven system (see also Rowan et al. (2004)).

4.7. Limiting factors

In a system driven by gravity, the stress field acting on the sediment is primarily a function of surface relief. Movement is resisted by the strength of the sediments and therefore sediment strength is also a factor, in particular strength of the detachment/décollement (see review of King and Morley (2017)). Many of the detachments in this study are interpreted to be dominated by overpressured shale or mudstone or have evidence for high pore fluid pressure/porosity based on seismic properties (Table 1), resulting in a relatively weak detachment. If the stress applied is reduced, the strength increases or the geometry changes in such a way as to increase the resistance, movement would decrease. If the resistance increases to the point that the stress is insufficient to move the sediment, movement will cease. Unless the geometry is changed in such a way as to increase the stress (through sediment deposition) (Table 2), or weaken the detachment, the system will remain frozen. Thus, the critical limiting factors are (1) stress and (2) strength of the detachment.

In a plate convergence-driven system, movement is also resisted by the strength of the sediments and detachment (Davis et al., 1983; Liu et al., 1992; Buiter, 2012; Ruh et al., 2012; Ruh et al., 2013). So if the geometry or material properties change in such a way that the stress is insufficient to move the sediments, the system will temporarily stop. However, the plates continue moving and the boundary of the FTB (detachment/décollement) continues moving at a rate determined by the plate convergence rate. In a locked system, this results in the stress increasing until the system breaks and the sediments once again move. We note that on a much shorter timescale, i.e. within the earthquake cycle of 100's years, stress applied does change through time. The impact of this effect on the Coulomb taper and stress regime within the forearc has

been analysed by Wang and Hu (2006). However, on the longer timescales covered by this study, these effects will not be observed. Thus, the plate-driven system is not limited by the strength of the materials involved in the FTB; the ultimate limiting factor is the rate at which the plate is fed into the FTB. On a large scale, the plate motion rate is effectively constant, and the plates will continue moving at the same speed over a long timescale. But the overall geometry and structure of the FTB will be affected by the properties of its internal and basal materials.

5. Conclusions

This study examines the geometry, structure and tectonic history of submarine fold-thrust belts induced by plate convergence, gravitational failure and a combined mechanism (hybrid system). The new results indicate the following:

1) The energy source in gravity-driven systems is within the sediment pile itself which is deformed to create upslope extension and downslope contraction, while in plate convergence driven systems, it is the movement of the stressed lithospheric-scale boundary, which lies outside the local sediment pile.
2) As a consequence, a prominent difference between the two systems is that the syn-kinematic sediments are thick (up to 6-7 km) and highly deformed (extensional faulting) in the gravity driven system, whereas they are thin (<0.5 km) and only slightly deformed (minor folding) in the plate-motion driven system. The thickening is attained by deposition of the syn-kinematic sequence in the gravity-driven system, whereas it is attained by shortening and stratigraphic repetition by thrusting in the plate convergence-driven system.
3) The energy in gravity-driven systems is resupplied by sediment inputs from large river deltas (Niger, Mississippi, Orange rivers, etc), and the timing of major episodes of movement is probably linked to major episodes of sediment input, likely controlled by climate. In a system driven by plate convergence, the energy is resupplied by movement of the plates and the plate boundary, which will continue regardless of sediment input.
4) The thrust faults of both systems are predominantly basinward-/seaward-verging imbricate thrusts detached onto a basal detachment. Backthrusts and back rotation appear to be only observed in the purely or predominantly plate convergence-driven fold-thrust belts. The anticlinal folds in both systems are dominated by asymmetric

fault-propagation folds (Figs. 3&12, Table 1) and many of the detachments appear to be weak and/or controlled by overpressured shale. This contrasts with the interpretation of Rowan et al. (2004) that asymmetric folds, and basinward-vergent imbricate thrusts develop above a strong basal detachment.

5) In gravity-driven systems, deformation in the extensional domain initiates on a small number of major listric faults and then becomes more distributed across multiple normal faults. In the contractional domain, for both driving mechanisms the fold-thrust belt propagates forward with new thrust initiation at the toe. However, fault activity differs slightly between the two systems; focused activity at the toe of the FTB is common for plate-driven systems but not observed in gravity-driven systems. Activity across much of the FTB is observed for both systems, but activity focused in the rear to middle of the FTB is only observed in gravity-driven FTB systems.
6) The rate of shortening across plate convergence-driven fold-thrust belts is orders of magnitude higher, and generally continuous on a long timescale. In contrast, within a gravity-driven system, the rate of shortening across the contractional domain is very slow and more variable through time.
7) In a system driven by gravity, the movement is resisted by the strength of the sediments and detachment. Thus, the critical limiting factors are stress and strength of the sediments/detachment. A plate-driven system is primarily limited by plate motion rate i.e, the rate at which the plate is fed into the FTB.

Figure captions:

Fig. 1. Conceptual cartoon showing fold-thrust belts driven by (a) plate convergence and (b) gravitational failure.

Fig. 2. Global map showing locations of submarine fold-thrust belts presented in this study. 1= Orange Basin, Namibia, 2= Para-Maranhao Basin, Brazil, 3= Amazon Fan, Brazil, 4= Niger Delta, Nigeria, 5= Nankai Accretionary Prism, Japan, 6= Hikurangi Accretionary Prism, New Zealand, 7= Makran Accretionary Prism, Iran, 8= NW Borneo, Brunei.

Fig. 3. Interpretation of a seismic reflection profile across the gravity-driven Orange Basin system, offshore Namibia, from the outer shelf to slope, after Granado et al. (2009), Morley et al. (2011) and Scarselli et al. (2016). The vertical exaggeration is 5. Interpreted units are stratigraphic sequences. This is regional seismic line vernab_03_063a

presented in Figure 2 of Granado et al. (2009)).

Fig. 4. Interpretation of a seismic profile showing architecture of the gravity-driven Para-Maranhao basin system, offshore Brazil, after Zalan et al. (2005); (Butler and Paton, 2010). The vertical exaggeration is 1.5. Interpreted units are structural sequences. The dashed lines represent approximated regional slopes of three sedimentary layers: top of Pre-kinematics, Growth I and Growth II. This is a cross-section presented in Fig. 1 of Butler and Paton (2010).

Fig. 5. Quantification of extensional and contractional deformation across the gravity-driven linked system, Para-Maranhao basin, offshore Brazil (Fig. 4). (a) Extensional area and contractional area constrained by estimated regional slope (see dashed lines in Fig. 4), interpreted faults and selected stratigraphic horizons, (b) plot of area of extension and contraction for each horizon, (c) plot of extensional and contractional strain magnitude for each horizon. Horizons 1-3 correspond to top of Pre-kinematic, Growth 1 and Growth II.

Fig. 6. (a) Interpretation of a seismic reflection profile across the gravity-driven Amazon Fan system, offshore Brazil from outer shelf to slope, after Cobbold et al. (2004), Morley et al. (2011). Interpreted units are stratigraphic sequences. The vertical exaggeration is 2. (b) Quantification of extension and contraction across this system using 3 stratigraphic horizons. Horizon 1 is the Top Cretaceous, Horizon 2 is the base Amazon fan, Horizon 3 is the Top Pliocene. This is the regional seismic profile 2 presented in Figure 2 of Cobbold et al. (2004)).

Fig. 7. Interpretation of a seismic reflection profile across the gravity-driven fold-thrust belt of the Niger Delta eastern lobe, Nigeria and Gulf of Guinea,
(after Ajakaiye and Bally (2002), Wu and McClay (2011)). No vertical exaggeration. Interpreted units are stratigraphic sequences. This is the line drawing of seismic profile D6A and D6B shown in Figure 2 of Ajakaiye and Bally (2002).

Journal Pre-proof

Fig. 8. Interpreted seismic reflection profile across the plate-convergence driven Nankai FTB system (Muroto transect), Japan, after Moore et al. (1990), Wu and McClay. (2011). The vertical exaggeration is 1.5. Interpreted units are stratigraphic sequences. This is seismic profile NT62-8 shown in Plate 1 of Moore et al. (1990).

Fig. 9. Interpreted seismic reflection profile across the the plate-convergence driven central Hikurangi FTB system, offshore North Island, New Zealand (after (Ghisetti et al. 2016)). Eight stratigraphic horizons are mapped with inferred age of 30+/5 Ma to present day. The vertical exaggeration is 2. Interpreted units are structural sequences. This is line SO-191-6, Transect 03 presented in Figure 5 of Ghisetti et al. (2016)

Fig. 10. Interpretation of a seismic reflection profile across the hybrid western Makran FTB and extensional system, offshore Iran. (a) Stratigraphy-based interpretation with stratigraphic sequences, (b) Structure-based interpretation with structural elements. The vertical exaggeration is 6. This is seismic line 2 shown in Figure 7 of Grando and McClay (2007).

Fig. 11. Plot of extension and contraction (heave only) across the hybrid Makran system for four stratigraphic horizons. Horizon 1 is top of Himalayan Turbidites, Horizon 2 is top of Makran Sands, Horizon 3 is top of Growth II, Horizon 4 is top of Growth III (Fig. 10a).

Fig. 12. Interpretation of a seismic reflection profile across the hybrid NW Borneo margin system. The profile shows extension in the shelf area and contraction beneath the slope. (a) Stratigraphy-based interpretation; (b) structure-based interpretation; c) schematic of the five stratigraphic units broken down across strike into tectonostratigraphic units for extension and contraction. Labels C, E and P represent contraction, extension, and post-kinematic, respectively. The vertical exaggeration is 3. This is the regional cross-section across Brunei based on seismic reflection data, shown in Figure 2 of Morley et al. (2014).

Journal Pre-proof

Bibliography

Ajakaiye, D.E. and Bally, A.W., 2002. Manual and atlas of structural styles on reflection profiles from the Niger Delta, AAPG Continuing Education Course Notes Series pp. 102.

Bally, A.W., Gordy, P.L. and Stewart, G.A., 1966. Structure, seismic data, and orogenic evolution of southern Canadian Rocky Mountains. Canadian Petroleum Geology Bulletin, 14: 337-381.

Bangs, N.L., Shipley, T.H., Gulick, S.P., Moore, G.F., Kuromoto, S. and Nakamura, Y., 2004. Evolution of the Nankai Trough décollement from the trench into the seismogenic zone: Inferences from three-dimensional seismic reflection imaging. Geology, 32(4): 273-276.

Barnes, P.M., de Lepinay, B.M., Collot, J.Y., Delteil, J. and Audru, J.C., 1998. Strain partitioning in the transition area between oblique subduction and continental collision, Hikurangi margin, New Zealand. Tectonics, 17(4): 534-557.

Barnes, P.M., Lamarche, G., Bialas, J., Henrys, S., Pecher, I., Netzeband, G.L., Greinert, J., Mountjoy, J.J., Pedley, K. and Crutchley, G., 2010. Tectonic and geological framework for gas hydrates and cold seeps on the Hikurangi subduction margin, New Zealand. Marine Geology, 272(1): 26-48.

Beavan, J., Tregoning, P., Bevis, M., Kato, T. and Meertens, C., 2002. Motion and rigidity of the Pacific Plate and implications for plate boundary deformation. Journal of Geophysical Research: Solid Earth, 107(B10): ETG 19-1-ETG 19-15.

Bilotti, F. and Shaw, J.H., 2005. Deep water Niger Delta fold and thrust belt modeled as a critical-taper wedge: The influence of elevated basal fluid pressure on structural styles. AAPG Bulletin, 89(11): 1475-1491.

Boyer, S.E. and Elliott, D., 1982. Thrust systems. AAPG Bulletin, 66(9): 1196-1230.

Buiter, S.J.H., 2012. A review of brittle compressional wedge models. Tectonophysics, 530: 1-17.

Burbank, D.W., Leland, J., Fielding, E., Anderson, R.S., Brozovic, N., Reid, M.R. and Duncan, C., 1996. Bedrock incision, rock uplift and threshold hillslopes in the northwestern Himalayas. Nature, 379(6565): 505.

Burg, J.-P., 2018. Geology of the onshore Makran accretionary wedge: Synthesis and tectonic interpretation. Earth-Science Reviews.

Burg, J.-P., Dolati, A., Bernoulli, D. and Smit, J., 2013. Structural style of the Makran Tertiary accretionary complex in SE-Iran, Lithosphere dynamics and sedimentary basins: The Arabian Plate and analogues. Springer, pp. 239-259.

Butler, R. and Paton, D., 2010. Evaluating lateral compaction in deepwater fold and thrust belts: How much are we missing from "nature's sandbox". GSA Today, 20(3): 4-10.

Butler, R.W.H. and Turner, J.P., 2010. Gravitational collapse at continental margins: products and processes; an introduction. Journal of the Geological Society, 167: 569-570.

Chapple, W.M., 1978. Mechanics of thin-skinned fold-and-thrust belts. Geological Society of America Bulletin, 89(8): 1189-1198.

Cobbold, P.R., Mourgues, R. and Boyd, K., 2004. Mechanism of thin-skinned detachment in the Amazon Fan: assessing the importance of fluid overpressure and hydrocarbon generation. Marine and petroleum geology, 21(8): 1013-1025.

Journal Pre-proof

Copley, A., Avouac, J.-P., Hollingsworth, J. and Leprince, S., 2011. The 2001 M-w 7.6 Bhuj earthquake, low fault friction, and the crustal support of plate driving forces in India. Journal of Geophysical Research-Solid Earth, 116: B08405.

Copley, A., Boait, F., Hollingsworth, J., Jackson, J. and McKenzie, D., 2009. Subparallel thrust and normal faulting in Albania and the roles of gravitational potential energy and rheology contrasts in mountain belts. Journal of Geophysical Research-Solid Earth, 114: B05407.

Corredor, F., Shaw, J.H. and Bilotti, F., 2005. Structural styles in the deep-water fold and thrust belts of the Niger Delta. AAPG Bulletin, 89(6): 753-780.

Coward, M.P., 1983. Thrust tectonics, thin skinned or thick skinned, and the continuation of thrusts to deep in the crust. Journal of Structural Geology, 5(2): 113-123.

Cruciani, F., Barchi, M., Koyi, H. and Porreca, M., 2017. Kinematic evolution of a regional-scale gravity-driven deepwater fold-and-thrust belt: The Lamu Basin case-history (East Africa). Tectonophysics, 712: 30-44.

Cruciani, F. and Barchi, M.R., 2016. The Lamu Basin deepwater fold-and-thrust belt: An example of a margin-scale, gravity-driven thrust belt along the continental passive margin of East Africa. Tectonics, 35(3): 491-510.

Dahlstrom, C., 1969. Balanced cross sections. Canadian Journal of Earth Sciences, 6(4): 743-757.

Dahlstrom, C.D., 1970. Structural geology in the eastern margin of the Canadian Rocky Mountains. Bulletin of Canadian Petroleum Geology, 18(3): 332-406.

Davis, D., Suppe, J. and Dahlen, F., 1983. Mechanics of fold-and-thrust belts and accretionary wedges. Journal of Geophysical Research: Solid Earth, 88(B2): 1153-1172.

Davis, D.M. and Engelder, T., 1985. The role of salt in fold-and-thrust belts. Tectonophysics, 119(1-4): 67-88.

DeMets, C., Gordon, R.G., Argus, D. and Stein, S., 1990. Current plate motions. Geophysical journal international, 101(2): 425-478.

DeMets, C., Gordon, R.G. and Argus, D.F., 2010. Geologically current plate motions. Geophysical Journal International, 181(1): 1-80.

DeMets, C., Gordon, R.G., Argus, D.F. and Stein, S., 1994. Effect of recent revisions to the geomagnetic reversal time scale on estimates of current plate motions. Geophysical research letters, 21(20): 2191-2194.

Diegel, F.A., Karlo, J., Schuster, D., Shoup, R. and Tauvers, P., 1995. Cenozoic structural evolution and tectono-stratigraphic framework of the northern Gulf Coast continental margin. In: M.P.A. Jackson, D.G. Roberts and S. Snelson (Editors), Salt tectonics: a global perspective:. AAPG Memoir pp. 109-151.

Doust, H. and Omatsola, E., 1989. Niger delta, Divergent/Passive Margin Basins. AAPG Memoir pp. 201-238.

Evamy, B., Haremboure, J., Kamerling, P., Knaap, W., Molloy, F. and Rowlands, P., 1978. Hydrocarbon habitat of Tertiary Niger delta. AAPG bulletin, 62(1): 1-39.

Fillon, C., Huismans, R. and van der Beek, P., 2012. Syntectonic sedimentation effects on the growth of fold and thrust belts. Geology, 41(1): 83-86.

Gerrard, I. and Smith, G., 1982. Post-Paleozoic succession and structure of the southwestern African continental margin, Studies in continental margin geology. American Association of Petroleum Geologists Memoir Tulsa, pp. 49-74.

Ghisetti, F.C., Barnes, P.M., Ellis, S., Plaza-Faverola, A.A. and Barker, D.H., 2016. The last 2 Myr of accretionary wedge construction in the central Hikurangi margin (North Island, New Zealand): Insights from structural modeling. Geochemistry, Geophysics, Geosystems, 17(7): 2661-2686.

Granado, P., De Vera, J. and McClay, K.R., 2009. Tectonostratigraphic evolution of the Orange Basin, SW Africa. Trabajos de geología, 29: 321-328.

Grando, G. and McClay, K., 2007. Morphotectonics domains and structural styles in the Makran accretionary prism, offshore Iran. Sedimentary Geology, 196(1-4): 157-179.

Gulick, S.P.S., Bangs, N.L.B., Shipley, T.H., Nakamura, Y., Moore, G. and Kuramoto, S., 2004. Three-dimensional architecture of the Nankai accretionary prism's imbricate thrust zone off Cape Muroto, Japan: Prism reconstruction via en echelon thrust propagation. Journal of Geophysical Research, 109(B2): B02105.

Haack, R.C., Sundararaman, P., Diedjomahor, J.O., Xiao, H., Gant, N.J., May, E.D. and Kelsch, K., 2000. Niger Delta petroleum systems, Nigeria. In: M.R. Mello and B.J. Katz (Editors), Petroleum systems of South Atlantic margins. AAPG Memoir 73, pp. 213-231.

Hales, T. and Roering, J.J., 2005. Climate-controlled variations in scree production, Southern Alps, New Zealand. Geology, 33(9): 701-704.

Hamilton, R. and De Vera, J., 2009. Review and global comparison of deepwater fold and thrust belt settings—Implications for their hydrocarbon prospectivity. Shell University Lecture Series.

Harms, J., Cappel, H. and Francis, D., 1984a. The Makran coast of Pakistan: its stratigraphy and hydrocarbon potential. Marine geology and oceanography of Arabian Sea and coastal Pakistan, 3: 27.

Harms, J.C., Cappel, H.N. and Francis, D.C., 1984b. The Makran coast of Pakistan: its stratigraphy and hydrocarbon potential. In: B.U. Haq and J.D. Milliman (Editors), Marine geology and oceanography of Arabian Sea and coastal Pakistan. Van Nostrand Reinhold, New York, pp. 3-26.

Hesse, S., Back, S. and Franke, D., 2009. The deep-water fold-and-thrust belt offshore NW Borneo: Gravity-driven versus basement-driven shortening. Geological Society of America Bulletin, 121(5-6): 939-953.

Hesse, S., Back, S. and Franke, D., 2010. Deepwater folding and thrusting offshore NW Borneo, SE Asia. Geological Society, London, Special Publications, 348(1): 169-185.

Higgins, S., Clarke, B., Davies, R.J. and Cartwright, J., 2009. Internal geometry and growth history of a thrust-related anticline in a deep water fold belt. Journal of Structural Geology, 31(12): 1597-1611.

Hills, D., Moore, G., Bangs, N. and Gulick, S., 2001. Preliminary Results from Integration of 2D PSDM and ODP Leg 196 LWD Velocity Data in the Nankai Accretionary Prism, AGU Fall Meeting San Francisco.

Hinz, K., Fritsch, J., Kempter, E.H.K., Mohammad, A.M., Meyer, J., Mohamed, D., Vosberg, H., Weber, J. and Benavidez, J., 1989. Thrust tectonics along the north-western continental margin of Sabah/Borneo. Geologische Rundschau, 78(3): 705-730.

Hosseini-Barzi, M. and Talbot, C.J., 2003. A tectonic pulse in the Makran accretionary prism recorded in Iranian coastal sediments. Journal of the Geological Society, 160(6): 903-910.

Journal Pre-proof

Ingram, G.M., Chisholm, T.J., Grant, C.J., Hedlund, C.A., Stuart-Smith, P. and Teasdale, J., 2004. Deepwater North West Borneo: Hydrocarbon accumulation in an active fold and thrust belt. Marine and Petroleum Geology, 21(7): 879-887.

King, R.C., Backe, G., Morley, C.K., Hillis, R.R. and Tingay, M.R.P., 2010a. Balancing deformation in NW Borneo: Quantifying plate-scale vs. gravitational tectonics in a delta and deepwater fold-thrust belt system. Marine and Petroleum Geology, 27(1): 238-246.

King, R.C., Hillis, R.R., Tingay, M.R.P. and Morley, C.K., 2010b. Present-day stress in Brunei, NW Borneo: Superposition of deltaic and active margin tectonics. Basin Research, 22: 236-247.

King, R.C. and Morley, C.K., 2017. Wedge geometry and detachment strength in deepwater fold-thrust belts. Earth-science reviews, 165: 268-279.

Koyi, H.A., Sans, M., Teixell, A., Cotton, J. and Zeyen, H., 2004. The significance of penetrative strain in the restoration of shortened layers—insights from sand models and the Spanish Pyrenees. In: K.R. McClay (Editor), Thrust tectonics and hydrocarbon systems. AAPG Memoir pp. 1-16.

Lathrop, B.A. and Burberry, C.M., 2017. Accommodation of penetrative strain during deformation above a ductile décollement. Lithosphere, 9(1): 46-57.

Light, M., Maslanyj, M., Greenwood, R. and Banks, N., 1993. Seismic sequence stratigraphy and tectonics offshore Namibia. Geological Society, London, Special Publications, 71(1): 163-191.

Liu, H.Q., McClay, K.R. and Powell, D., 1992. Physical models of thrust wedges. In: K.R. McClay (Editor), Thrust Tectonics. Chapman and Hall, London, pp. 71-81.

Lohr, T., Krawczyk, C., Tanner, D., Samiee, R., Endres, H., Thierer, P., Oncken, O., Trappe, H., Bachmann, R. and Kukla, P., 2008. Prediction of sub-seismic faults and fractures: integration of 3D seismic data, 3D retrodeformation, and well data on an example of deformation around an inverted fault. AAPG Bulletin, 92(4): 473-485.

Loveless, J.P. and Meade, B.J., 2010. Geodetic imaging of plate motions, slip rates, and partitioning of deformation in Japan. Journal of Geophysical Research: Solid Earth, 115(B2).

MacKay, M.E., Moore, G.F., Cochrane, G.R., Moore, J.C. and Kulm, L.D., 1992. Landward vergence and oblique structural trends in the Oregon margin accretionary prism: Implications and effect on fluid flow. Earth and Planetary Science Letters, 109(3-4): 477-491.

McNeill, L.C. and Henstock, T.J., 2014. Forearc structure andmorphology along the SumatraAndaman subduction zone. Tectonics, 33(2): 112-134.

McNeill, L.C., Piper, K.A., Goldfinger, C., Kulm, L.D. and Yeats, R.S., 1997. Listric normal faulting on the Cascadia continental margin. Journal of Geophysical Research: Solid Earth, 102(B6): 12123-12138.

Mello, M.R., Azambuja, N., Mohriak, W., Catto, A. and Françolin, J., 2011. Promising giant new hydrocarbon frontier: the Namibian continental margin. GEOEXPRO, 8(6): 64-66.

Moore, G.F. and Curray, J.R., 1980. Structure of the Sunda Trench lower slope off Sumatra from multichannel seismic reflection data. Marine Geophysical Researches, 4(3): 319-340.

Moore, G.F., Shipley, T., Stoffa, P., Karig, D., Taira, A., Kuramoto, S., Tokuyama, H. and Suyehiro, K., 1990. Structure of the Nankai Trough accretionary zone from

multichannel seismic reflection data. Journal of Geophysical Research: Solid Earth, 95(B6): 8753-8765.

Moore, G.F., Taira, A., Klaus, A., Becker, L., Boeckel, B., Cragg, B.A., Dean, A., Fergusson, C.L., Henry, P. and Hirano, S., 2001. New insights into deformation and fluid flow processes in the Nankai Trough accretionary prism: Results of Ocean Drilling Program Leg 190. Geochemistry, Geophysics, Geosystems, 2(10): 2001GC000166.

Moore, J.C. and Saffer, D., 2001. Updip limit of the seismogenic zone beneath the accretionary prism of southwest Japan: An effect of diagenetic to low-grade metamorphic processes and increasing effective stress. Geology, 29(2): 183-186.

Moore, J.C. and Silver, E.A., 1987. Continental margin tectonics: Submarine accretionary prisms. Reviews of Geophysics, 25(6): 1305-1312.

Morgan, J.K. and Karig, D.E., 1995. Kinematics and a balanced and restored cross-section across the toe of the eastern Nankai accretionary prism. Journal of Structural Geology, 17(1): 31-45.

Morley, C. and Guerin, G., 1996. Comparison of gravity-driven deformation styles and behavior associated with mobile shales and salt. Tectonics, 15(6): 1154-1170.

Morley, C.K., 2003. Mobile shale related deformation in large deltas developed on passive and active margins. In: P. VanRensbergen, R.R. Hillis, A.J. Maltman and C.K. Morley (Editors), Subsurface Sediment Mobilization. Geological Society Special Publication, pp. 335-357.

Morley, C.K., 2007. Interaction between critical wedge geometry and sediment supply in a deep water fold belt. Geology, 35(2): 139-142.

Morley, C.K., King, R., Hillis, R., Tingay, M. and Backe, G., 2011. Deepwater fold and thrust belt classification, tectonics, structure and hydrocarbon prospectivity: A review. Earth-Science Reviews, 104(1-3): 41-91.

Morley, C.K., Warren, J., Tingay, M., Boonyasaknanon, P. and Julapour, A., 2014. Reprint of: Comparison of modern fluid distribution, pressure and flow in sediments associated with anticlines growing in deepwater (Brunei) and continental environments (Iran). Marine and petroleum geology, 55: 230-249.

Peach, B.N., Horne, J., Gunn, W., Clough, C.T., Teall, J.J.H. and Hinxman, L.W., 1907. The geological structure of the North-West Highlands of Scotland. HM Stationery Office, Glasgow.

Peel, F.J., 2014. The engines of gravity-driven movement on passive margins: Quantifying the relative contribution of spreading vs. gravity sliding mechanisms. Tectonophysics, 633: 126-142.

Peel, F.J., Travis, C.J. and Hossack, J.R., 1995. Genetic structural provinces and salt tectonics of the Cenozoic offshore US Gulf of Mexico: A preliminary analysis. In: M.P.A. Jackson, D.G. Roberts and S. Snelson (Editors), Salt Tectonics: A Global Perspective. AAPG MEMOIR, pp. 153-175.

Price, R. and Mountjoy, E., 1970. Geologic structure of the Canadian Rocky Mountains between Bow and Athabasca Rivers—a progress report. Geological Association of Canada Special Paper, 6: 7-25.

Ranero, C.R. and von Huene, R., 2000. Subduction erosion along the Middle America convergent margin. Nature, 404(6779): 748.

Riebe, C.S., Sklar, L.S., Lukens, C.E. and Shuster, D.L., 2015. Climate and topography control the size and flux of sediment produced on steep mountain slopes. Proceedings of the National Academy of Sciences, 112(51): 15574-15579.

Journal Pre-proof

Rodgers, J., 1949. Evolution of thought on structure of middle and southern Appalachians. American Association of Petroleum Geologists Bulletin, 33: 1643-1654.

Rowan, M.G., Peel, F.J. and Vendeville, B.C., 2004. Gravity-driven Fold Belts on passive margins. In: K.R. McClay (Editor), Thrust tectonics and hydrocarbon systems. AAPG Memoir 82, pp. 157-182.

Rowan, M.G., Trudgill, B.D. and Fiduk, J.C., 2000. Deep-water, salt-cored foldbelts: Lessons from the Mississippi Fan and Perdido foldbelts, northern Gulf of Mexico. Atlantic Rifts and Continental Margins, 115: 173-191.

Ruh, J.B., Gerya, T. and Burg, J.P., 2013. High-resolution 3D numerical modeling of thrust wedges: Influence of décollement strength on transfer zones. Geochemistry, Geophysics, Geosystems, 14(4): 1131-1155.

Ruh, J.B., Kaus, B.J.P. and Burg, J.-P., 2012. Numerical investigation of deformation mechanics in fold-and-thrust belts: Influence of rheology of single and multiple decollements. Tectonics, 31: TC3005.

Sans, M., Vergés, J., Gomis, E., Parés, J., Schiattarella, M., Travé, A., Calvet, F., Santanach, P. and Doulcet, A., 2003. Layer parallel shortening in salt detached folds: constraint on cross-section restoration. Tectonophysics, 372(1-2): 85-104.

Sapin, F., Hermawan, I., Pubellier, M., Vigny, C. and Ringenbach, J.C., 2013. The recent convergence on the NW Borneo Wedge-a crustal-scale gravity gliding evidenced from GPS. Geophysical Journal International, 193(2): 549-556.

Sapin, F., Pubellier, M., Lahfid, A., Janots, D., Auxbourg, C. and Ringenbach, J.C., 2011. Onshore record of the subduction of a crustal salient: example of the NW Borneo Wedge. Terra Nova, 23(4): 232-240.

Scarselli, N., McClay, K. and Elders, C., 2016. Seismic geomorphology of Cretaceous megaslides offshore Namibia (Orange Basin): insights into segmentation and degradation of gravity-driven linked systems. Marine and Petroleum Geology, 75: 151-180.

Şengör, A.C. and Bozkurt, E., 2013. Layer-parallel shortening and related structures in zones undergoing active regional horizontal extension. International Journal of Earth Sciences, 102(1): 101-110.

Seno, T., Stein, S. and Gripp, A.E., 1993. A model for the motion of the Philippine Sea plate consistent with NUVEL-1 and geological data. Journal of Geophysical Research: Solid Earth, 98(B10): 17941-17948.

Séranne, M. and Anka, Z., 2005. South Atlantic continental margins of Africa: a comparison of the tectonic vs climate interplay on the evolution of equatorial west Africa and SW Africa margins. Journal of African Earth Sciences, 43(1-3): 283-300.

Shaw, J.H., Connors, C.D. and Suppe, J., 2005. Seismic interpretation of contractional fault-related folds: An AAPG seismic atlas. American Association of Petroleum Geologists, pp. 1-157.

Simons, W.J.F., Socquet, A., Vigny, C., Ambrosius, B.A.C., Abu, S.H., Promthong, C., Subarya, C., Sarsito, D.A., Matheussen, S., Morgan, P. and Spakman, W., 2007. A decade of GPS in Southeast Asia: Resolving Sundaland motion and boundaries. Journal of Geophysical Research-Solid Earth, 112: B06420.

Smith, G., McNeill, L., Henstock, T.J. and Bull, J., 2012. The structure and fault activity of the Makran accretionary prism. Journal of Geophysical Research-Solid Earth, 117: B07407.

Journal Pre-proof

Storti, F. and McClay, K., 1995. Influence of syntectonic sedimentation on thrust wedges in analogue models. Geology, 23(11): 999-1002.

Trudgill, B.D., Fiduk, J.C., Weimer, P., Rowan, M.G., Gale, P.E., Korn, B.E., Phair, R.L., Gafford, W.T., Dischinger, J.B., Roberts, G.R. and Henage, L.F., 1995. The geological evolution of the deep water Perdido Foldbelt, Alaminos Canyon, northwestern deep Gulf of Mexico. . Gulf Coast Association of Geological Societies Transactions, 45: 573-579.

Trudgill, B.D., Rowan, M.G., Fiduk, J.C., Weimer, P., Gale, P.E., Korn, B.E., Phair, R.L., Gafford, W.T., Roberts, G.R. and Dobbs, S.W., 1999. The perdido fold belt, northwestern deep gulf of mexico, part 1: Structural geometry, evolution and regional implications1. AAPG bulletin, 83(1): 88-113.

Van Rensbergen, P. and Morley, C.K., 2003. Re-evaluation of mobile shale occurrences on seismic sections of the Champion and Baram deltas, offshore Brunei. In: P. VanRensbergen, R.R. Hillis, A.J. Maltman and C.K. Morley (Editors), Subsurface Sediment Mobilization. Geological Society Special Publication, pp. 395-409.

Vernant, P., Nilforoushan, F., Hatzfeld, D., Abbassi, M., Vigny, C., Masson, F., Nankali, H., Martinod, J., Ashtiani, A. and Bayer, R., 2004. Present-day crustal deformation and plate kinematics in the Middle East constrained by GPS measurements in Iran and northern Oman. Geophysical Journal International, 157(1): 381-398.

Von Huene, R., 1979. Structure of the Outer Convergent Margin Off Kodiak Island, Alaska, from Multichannel Seismic Records: Convergent Margins.

von Huene, R. and Scholl, D.W., 1991. OBSERVATIONS AT CONVERGENT MARGINS CONCERNING SEDIMENT SUBDUCTION, SUBDUCTION EROSION, AND THE GROWTH OF CONTINENTAL-CRUST. Reviews of Geophysics, 29(3): 279-316.

Walcott, R., 1998. Modes of oblique compression: Late Cenozoic tectonics of the South Island of New Zealand. Reviews of geophysics, 36(1): 1-26.

Wallace, L.M., Reyners, M., Cochran, U., Bannister, S., Barnes, P.M., Berryman, K., Downes, G., Eberhart-Phillips, D., Fagereng, A. and Ellis, S., 2009. Characterizing the seismogenic zone of a major plate boundary subduction thrust: Hikurangi Margin, New Zealand. Geochemistry, Geophysics, Geosystems, 10(10): Q10006.

Wang, C., Chen, H., Cheng, X. and Li, K., 2013. Evaluating the role of syn-thrusting sedimentation and interaction with frictional detachment in the structural evolution of the SW Tarim Basin, NW China : Insights from analogue modeling Tectonophysics, 608: 642-652.

Wang, K. and Hu, Y., 2006. Accretionary prisms in subduction earthquake cycles: The theory of dynamic Coulomb wedge. Journal of Geophysical Research-Solid Earth, 111: B06410.

Weimer, P. and Buffler, R.T., 1992. Structural Geology and Evolution of the Mississippi Fan Fold Belt, Deep Gulf of Mexico (1). AAPG Bulletin, 76(2): 225-251.

Westbrook, G.K., 1975. The structure of the crust and upper mantle in the region of Barbados and the Lesser Antilles. Geophysical Journal International, 43(1): 201-242.

Westbrook, G.K., Ladd, J.W., Buhl, P., Bangs, N. and Tiley, G.J., 1988. Cross section of an accretionary wedge: Barbados Ridge complex. Geology, 16(7): 631-635.

Westbrook, G.K., Smith, M.J., Peacock, J.H. and Poulter, M.J., 1982. Extensive underthrusting of undeformed sediment beneath the accretionary complex of the Lesser Antilles subduction zone. Nature, 300(5893): 625-628.

Whipple, K.X., Kirby, E. and Brocklehurst, S.H., 1999. Geomorphic limits to climate-induced increases in topographic relief. Nature, 401(6748): 39.

White, R.S., 1982. Deformation of the Makran accretionary sediment prism in the Gulf of Oman (north-west Indian Ocean). Geological Society, London, Special Publications, 10(1): 357-372.

White, R.S. and Louden, K.E., 1982. The Makran Continental Margin: Structure of a Thickly Sedimented Convergent Plate Boundary: Convergent Margins: Field Investigations of Margin Structure and Stratigraphy. In: J.S. Watkins and C.L. Drake (Editors), Studies in Continental Margin Geology. American Association of Petroleum Geologists Memoir, Tulsa, OK, USA, pp. 499-518.

Wickens, H.d.V. and McLachlan, I., 1990. The stratigraphy and sedimentology of the reservoir interval of the Kudu 9A-2 and 9A-3 boreholes. Communications of the Geological Survey of Namibia, 6: 9-22.

Wu, J.E., McClay, K. and Frankowicz, E., 2015. Niger Delta gravity-driven deformation above the relict Chain and Charcot oceanic fracture zones, Gulf of Guinea: Insights from analogue models. Marine and Petroleum Geology, 65: 43-62.

Wu, J.E. and McClay, K.R., 2011. Two-dimensional analog modelling of fold and thrust belts: dynamic interactions with syncontractional sedimentation and erosion AAPG Bulletin, 94: 301-333.

Wu, S., Bally, A.W. and Cramez, C., 1990. Allochthonous salt, structure and stratigraphy of the north-eastern Gulf of Mexico. Part II: Structure. Marine and Petroleum Geology, 7(4): 334-370.

Zalan, P., Shaw, J., Connors, C. and Suppe, J., 2005. End members of gravitational fold and thrust belts (GFTBs) in the deep waters of Brazil. An AAPG Seismic Atlas: AAPG Studies in Geology, 53: 147-156.

Journal Pre-proof

Table 1 The parameters of fold-thrust belt examples used in this study.

	Parameters										
Width W (km)	**W_E (km)**	**W_C (km)**	**W_T (km)**	**Thickness, T_H (km)**	**T_F (km)**	**Detachment dip and properties**	**Extension (km)**	**Shortening (km)**	**Shortening /Convergence Rate (mm/yr)**	**Faults**	**Folds**
55	133	84	4	3.7 s	2.3 s	gently seaward dipping overpressured shale			2.3-2.6	dominant regional listric normal faults seaward-verging imbricate thrusts	asymmetric fault propagation folds (FPFs)
3	20	16	0	2.7	2.0	gently seaward dipping overpressured mudstone	3.0-14.4	0.2-4.2	0.8	a major and several small regional listric normal faults seaward-verging imbricate thrusts	asymmetric FPFs
32	131	90	11	10.1	8.0	gently seaward dipping overpressured and compacted shale	1.8-18.5	0.9-14		dominant regional and few counter regional listric normal faults seaward-verging imbricate thrusts	asymmetric FPFs
03	93	69	41	6.4 s	2.2 s	Gently seaward dipping at extension and landward dipping at contraction, overpressured and compacted shale		17-25	1.4-2.0	Two major Listric regional and counter regional listric faults and a number of rootless planar normal faults seaward-verging imbricate thrusts	Asymmetric FPFs
7	0	21	0	2.0	0.9	6-8° landward dipping overpressured mudstone/shale			40-60	Seaward-verging imbricate thrusts a few landward-verging thrusts	Asymmetric FPFs

Journal Pre-proof

9		55		6.4	2.9	Moderately landward dipping weak detachment?		16.6	19-61	Dominant seaward-verging listric and planar imbricate thrusts and a few planar backthrusts, splay faults	Asymmetric FPFs
78	47	85	20.4	7.6 s	2.7 s	1-3° landward dipping, weak detachment?	0.5-3.8	0.4-33.2	27-42	A major listric normal fault, several rootless planar normal faults dominant seaward-verging imbricate thrusts, two planar backthrusts	Asymmetric FPFs
131	46 45.9	85	80.4	800	2.5-3	Gently landward dipping, Overpressured shale	0.5-6	4-7	4-6	A few major counter regional listric normal faults, many rootless planar normal faults, dominant seaward-verging imbricate thrusts, two rootless planar backthrust	Asymmetric FPFs

W=Width of whole cross section, W_E=width of extension, W_C= width of contraction, T_H=thickness of upslope or hinterland, T_F=Thickness of foreland, E= extension, S= shortening, SR= shortening rate. Please note for time sections, the thickness is measured in seconds (two way time), so the value is followed by unit s.

Journal Pre-proof

Table 2. The characteristics of the fold-thrust belts relative to system type/driving mechanism.

PARAMETER	PLATE CONVERGENCE	GRAVITY
Energy	Gravitational PE within the crust/lithosphere outside the local deforming sediment pile	Gravitational potential energy (PE) contained within the deforming sediment pile itself
Control on state of stress	Tectonic shortening rate, strength of décollement	Surface slope (controlled by depositional processes)
Detachment dip direction	Landward	Variable; mostly gently basinward, sometimes landward
Surface slope	1-6°	1-4°
Strain localization	Imbricate thrusts	Major listric extensional faults and imbricate thrusts
Fault vergence	Seaward dominant, landward also observed	Seaward
Back thrusts	A few	No
Back rotation of thrusts	Yes	No
Seafloor deformation	Large (significant folding and thrusting)	Minor or negligible (slight folding only)
History	Contraction only Forward propagation of thrust activation. Activity typically focused at the toe or across belt	Extension leading to contraction Forward propagation of thrust activation. Activity across wide zone of fold-thrust belt
Net contraction	High	Low
Overall convergence/ shortening rate	High (several cm's per year), constant	Low (a few mm's per year), pulsed

Journal Pre-proof

Journal Pre-proof

3rd February, 2020

To whom it may concern,

We declare there is no conflict of interest within this study.

Yours sincerely

Xiaodong Yang (email: yang@ipgp.fr)

Journal Pre-proof

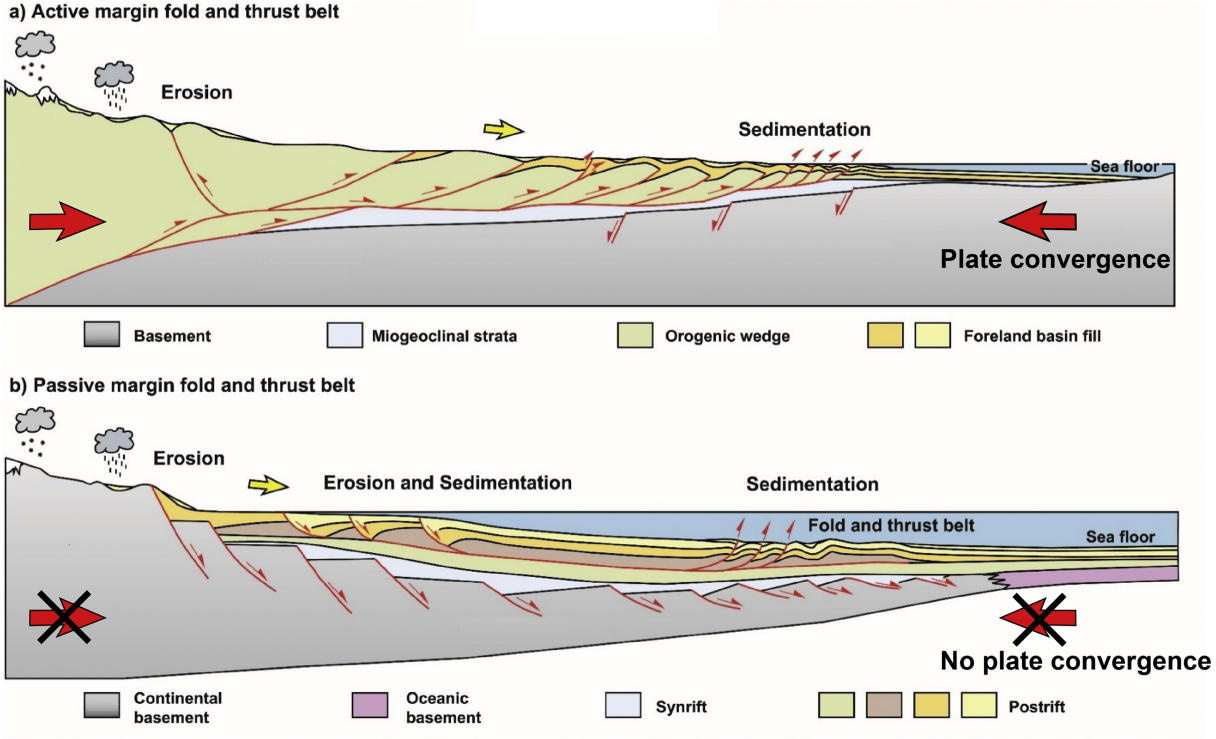
a) Active margin fold and thrust belt
Erosion
Sedimentation
Sea floor
Plate convergence
Basement
Miogeoclinal strata
Orogenic wedge
Foreland basin fill
b) Passive margin fold and thrust belt
Erosion
Erosion and Sedimentation
Sedimentation
Fold and thrust belt
Sea floor
No plate convergence
Continental basement
Oceanic basement
Synrift
Postrift

Figure 1

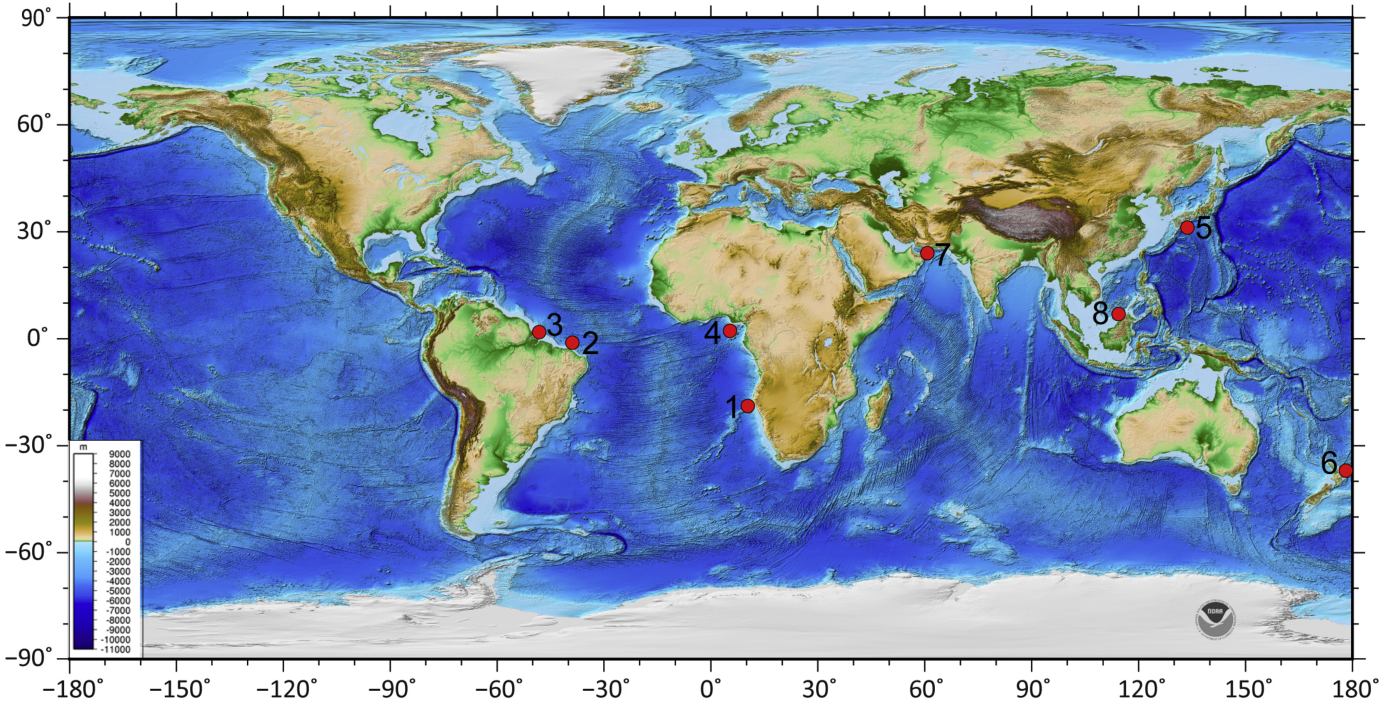
90°
60°
30°
0°
−30°
−60°
−90°
−180°
−150°
−120°
−90°
−60°
−30°
0°
30°
60°
90°
120°
150°
180°
1
2
3
4
5
6
7
8
m
9000
8000
7000
6000
5000
4000
3000
2000
1000
0
-1000
-2000
-3000
-4000
-5000
-6000
-7000
-8000
-9000
-10000
-11000

Figure 2

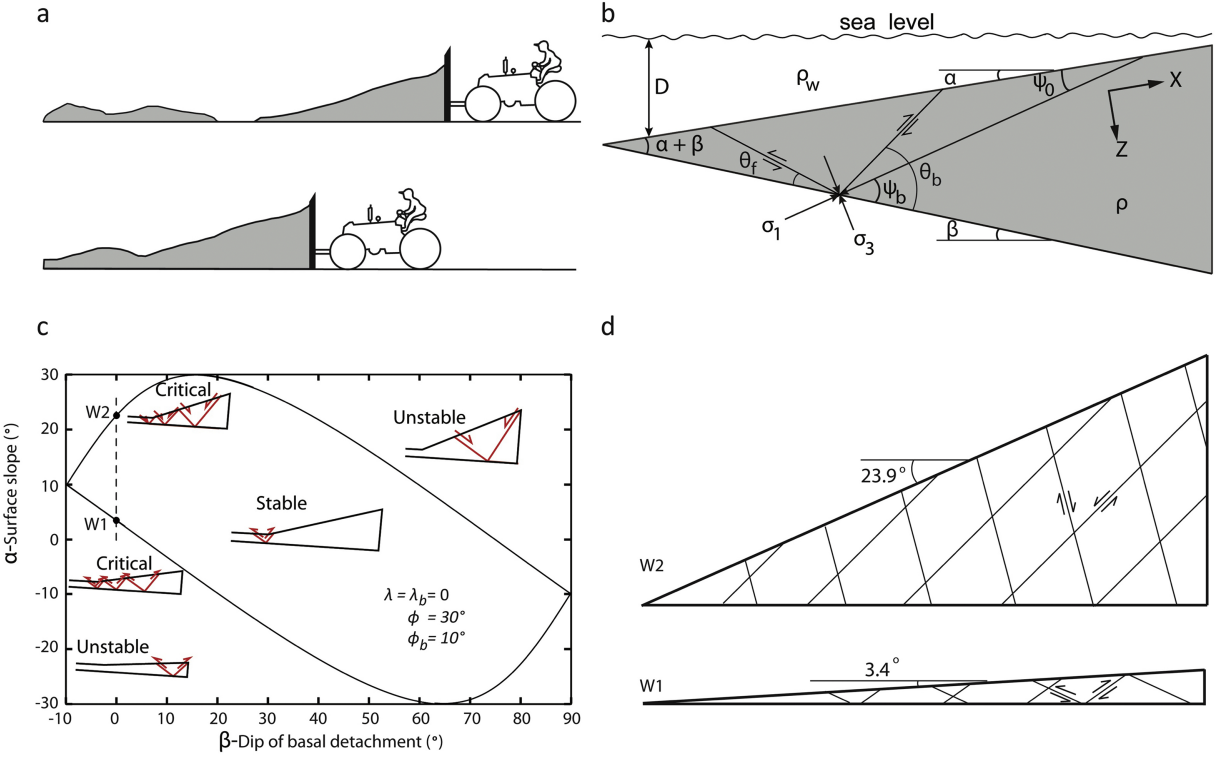
a
b
sea level
D
ρ_w
α
ψ_0
X
Z
α + β
θ_f
θ_b
ψ_b
ρ
σ_1
σ_3
β
c
d
Critical
W2
Unstable
Stable
W1
Critical
Unstable
λ = λ_b= 0
ϕ = 30°
ϕ_b= 10°
α-Surface slope (°)
β-Dip of basal detachment (°)
23.9°
W2
3.4°
W1

Figure 3

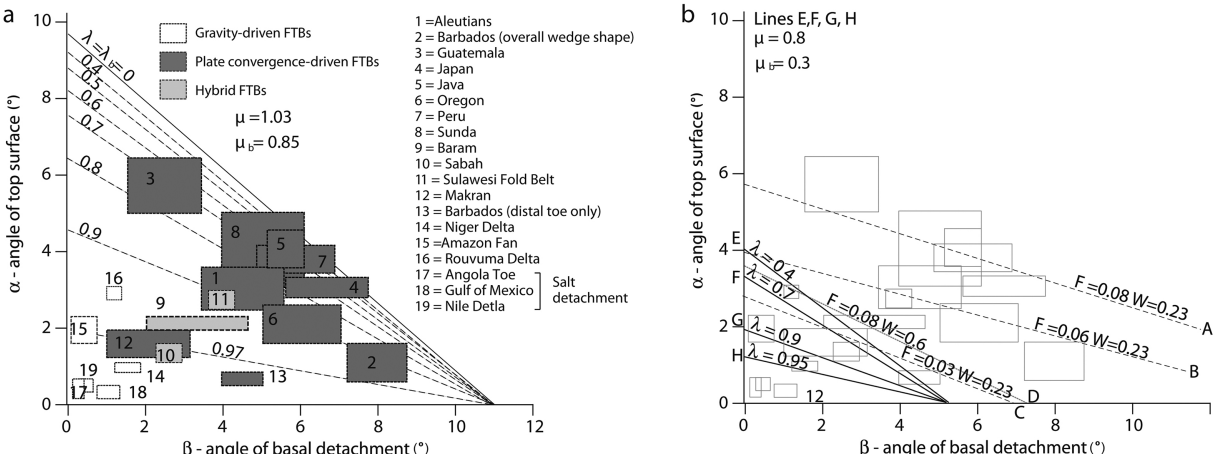
a
α - angle of top surface (°)
β - angle of basal detachment (°)
Gravity-driven FTBs
Plate convergence-driven FTBs
Hybrid FTBs
μ =1.03
μ b= 0.85
λ =λ b= 0
0.4
0.5
0.6
0.7
0.8
0.9
0.97
1 =Aleutians
2 = Barbados (overall wedge shape)
3 = Guatemala
4 = Japan
5 = Java
6 = Oregon
7 = Peru
8 = Sunda
9 = Baram
10 = Sabah
11 = Sulawesi Fold Belt
12 = Makran
13 = Barbados (distal toe only)
14 = Niger Delta
15 =Amazon Fan
16 = Rouvuma Delta
17 = Angola Toe
18 = Gulf of Mexico
19 = Nile Detla
Salt detachment
b
Lines E,F, G, H
μ = 0.8
μ b= 0.3
α - angle of top surface (°)
β - angle of basal detachment (°)
E
F
G
H
λ = 0.4
λ = 0.7
λ = 0.9
λ = 0.95
F =0.08 W=0.23
F =0.08 W=0.6
F =0.06 W=0.23
F =0.03 W=0.23
A
B
C
D

Figure 4

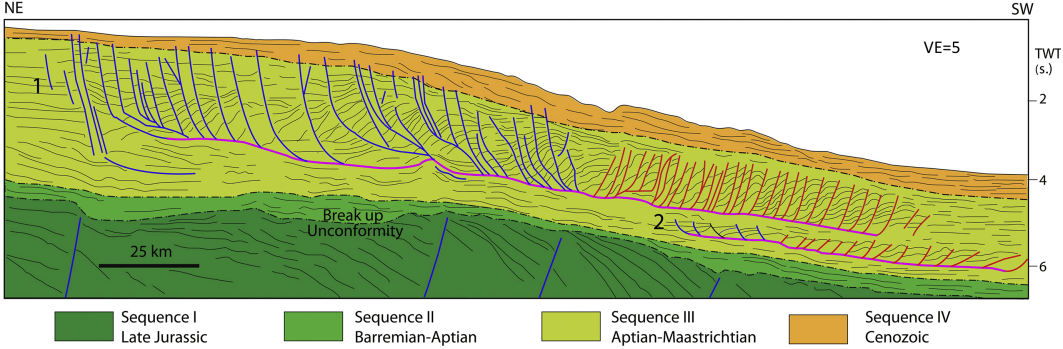
NE
SW
VE=5
TWT
(s.)
2
4
6
1
2
Break up
Unconformity
25 km
Sequence I
Late Jurassic
Sequence II
Barremian-Aptian
Sequence III
Aptian-Maastrichtian
Sequence IV
Cenozoic

Figure 5

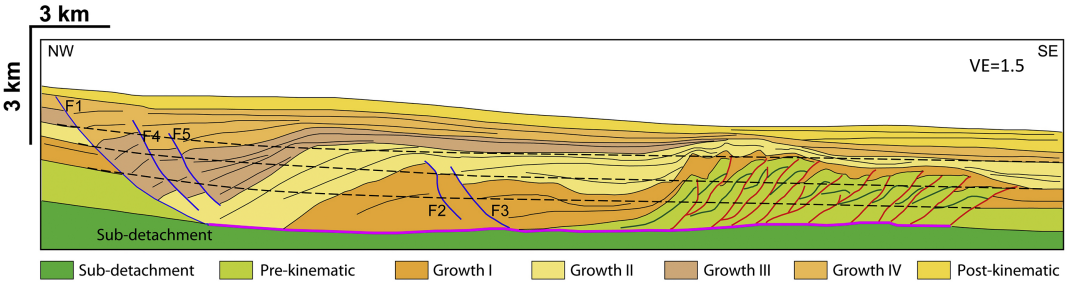
3 km
3 km
NW
SE
VE=1.5
F1
F4
F5
F2
F3
Sub-detachment
Sub-detachment
Pre-kinematic
Growth I
Growth II
Growth III
Growth IV
Post-kinematic

Figure 6

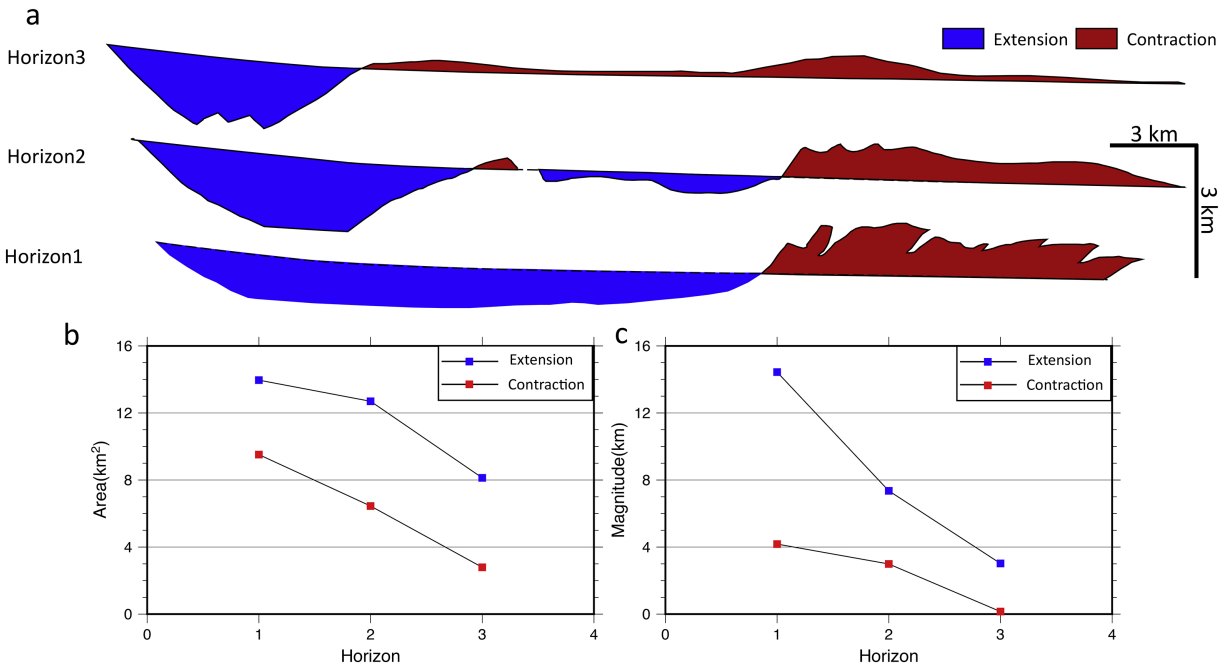
a
Horizon3
Horizon2
Horizon1
Extension
Contraction
3 km
3 km
b
Area(km²)
Horizon
Extension
Contraction
c
Magnitude(km)
Horizon
Extension
Contraction

Figure 7

a

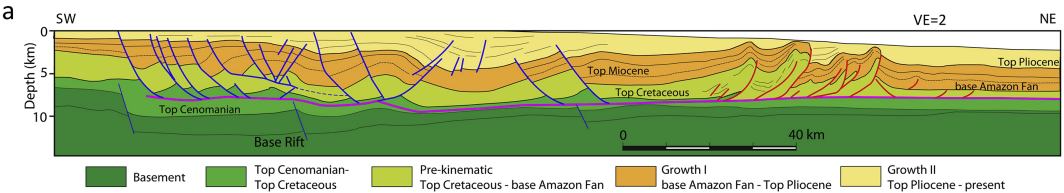
SW
NE
VE=2
Depth (km)
0
5
10
Top Pliocene
Top Miocene
Top Cretaceous
base Amazon Fan
Top Cenomanian
Base Rift
0
40 km
Basement
Top Cenomanian-
Top Cretaceous
Pre-kinematic
Top Cretaceous - base Amazon Fan
Growth I
base Amazon Fan - Top Pliocene
Growth II
Top Pliocene - present

b

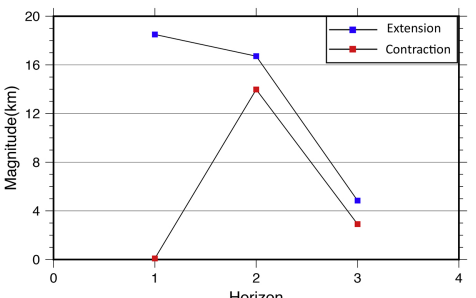
Extension
Contraction
Magnitude(km)
20
16
12
8
4
0
0
1
2
3
4
Horizon

Figure 8

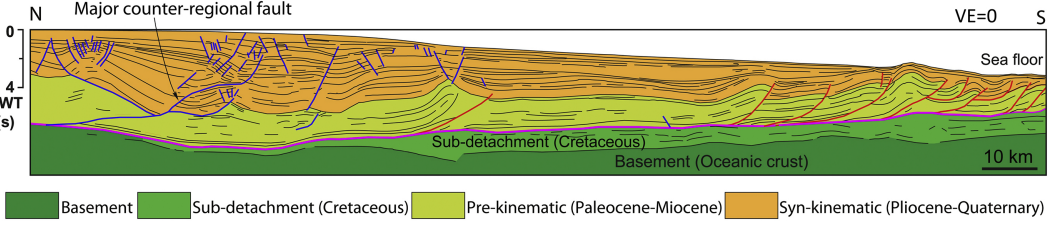
N
Major counter-regional fault
VE=0
S
0
4
TWT
(s)
Sea floor
Sub-detachment (Cretaceous)
Basement (Oceanic crust)
10 km
Basement
Sub-detachment (Cretaceous)
Pre-kinematic (Paleocene-Miocene)
Syn-kinematic (Pliocene-Quaternary)

Figure 9

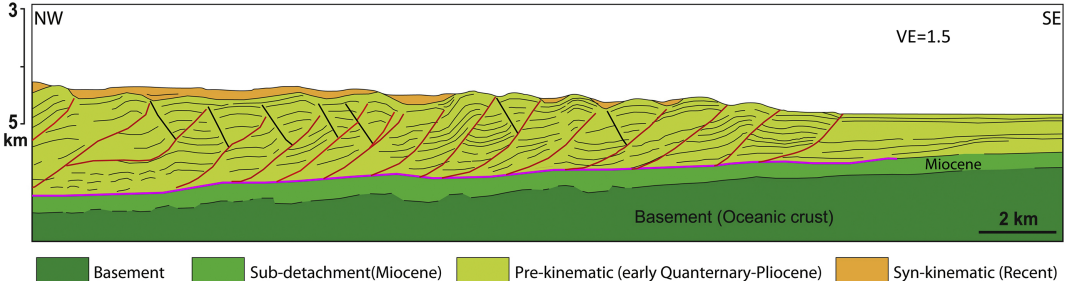
3
NW
SE
VE=1.5
5
km
Miocene
Basement (Oceanic crust)
2 km
Basement
Sub-detachment(Miocene)
Pre-kinematic (early Quanternary-Pliocene)
Syn-kinematic (Recent)

Figure 10

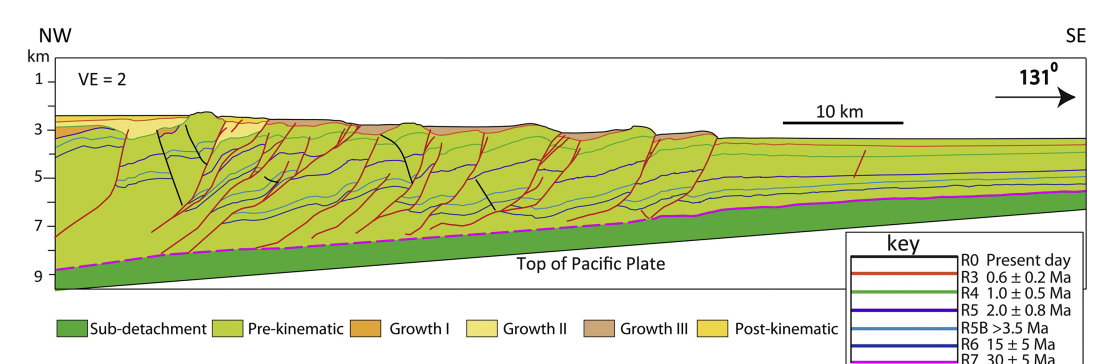
NW
SE
km
1
3
5
7
9
VE = 2
131°
10 km
Top of Pacific Plate
key
R0 Present day
R3 0.6 ± 0.2 Ma
R4 1.0 ± 0.5 Ma
R5 2.0 ± 0.8 Ma
R5B >3.5 Ma
R6 15 ± 5 Ma
R7 30 ± 5 Ma
Sub-detachment
Pre-kinematic
Growth I
Growth II
Growth III
Post-kinematic

Figure 11

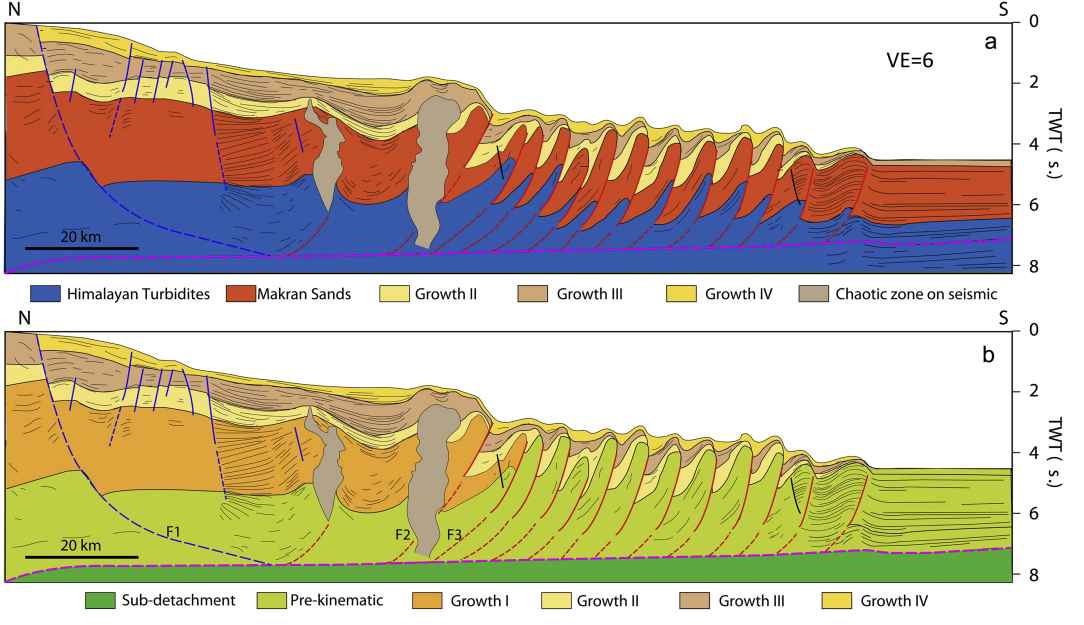
N
S
a
VE=6
0
2
4
6
8
TWT (s.)
20 km
Himalayan Turbidites
Makran Sands
Growth II
Growth III
Growth IV
Chaotic zone on seismic
N
S
b
0
2
4
6
8
TWT (s.)
20 km
F1
F2
F3
Sub-detachment
Pre-kinematic
Growth I
Growth II
Growth III
Growth IV

Figure 12

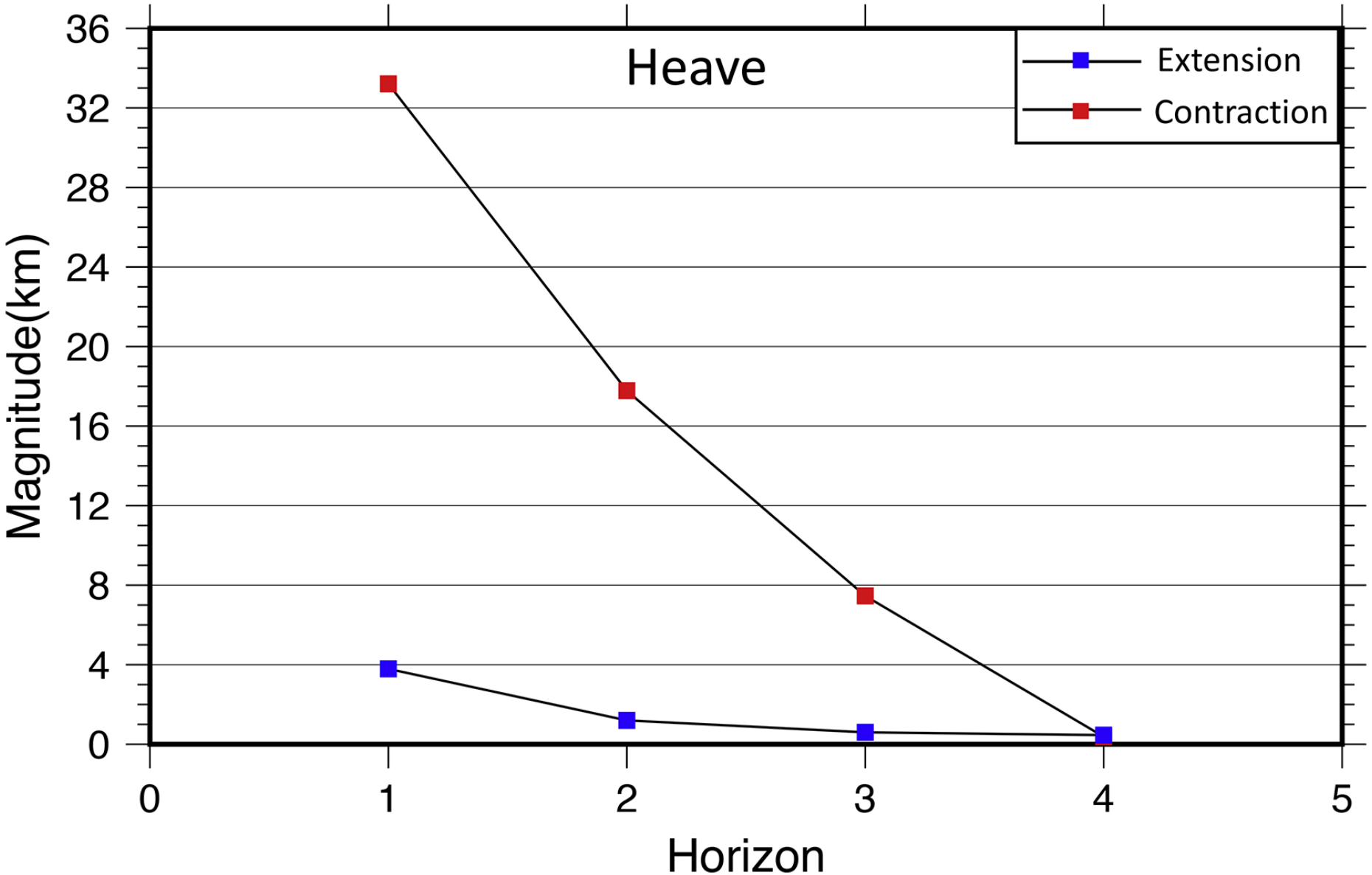
Heave
Extension
Contraction
Magnitude(km)
36
32
28
24
20
16
12
8
4
0
0
1
2
3
4
5
Horizon

Figure 13

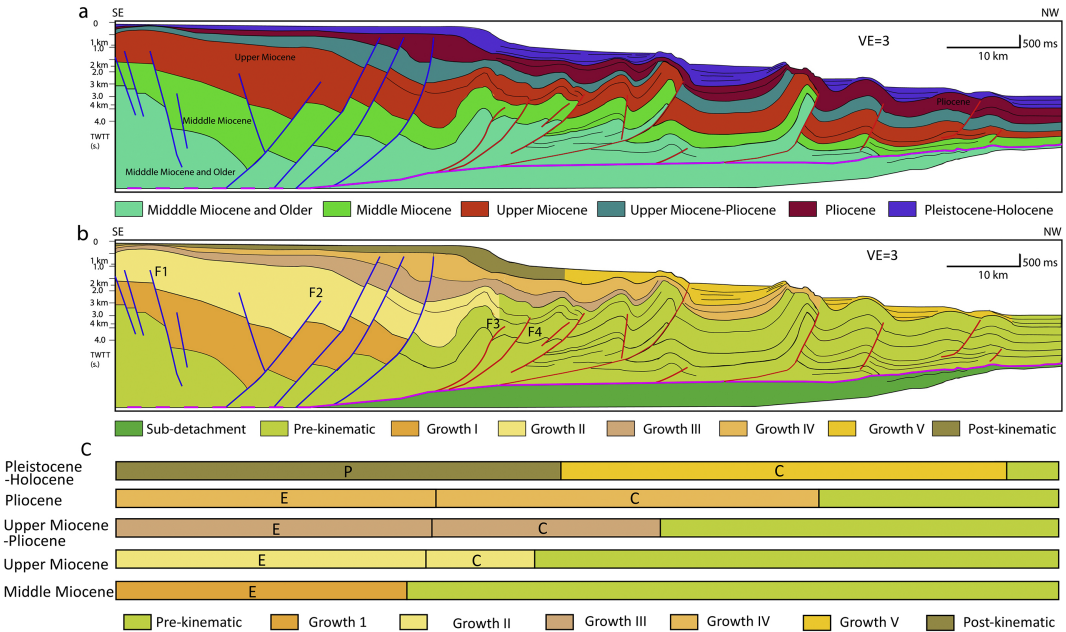
a
SE
NW
VE=3
500 ms
10 km
Upper Miocene
Middle Miocene
Middle Miocene and Older
Pliocene
TWTT (s.)
Middle Miocene and Older
Middle Miocene
Upper Miocene
Upper Miocene-Pliocene
Pliocene
Pleistocene-Holocene
b
SE
NW
VE=3
500 ms
10 km
F1
F2
F3
F4
TWTT (s.)
Sub-detachment
Pre-kinematic
Growth I
Growth II
Growth III
Growth IV
Growth V
Post-kinematic
C
Pleistocene -Holocene
Pliocene
Upper Miocene -Pliocene
Upper Miocene
Middle Miocene
P
C
E
C
E
C
E
C
E
Pre-kinematic
Growth 1
Growth II
Growth III
Growth IV
Growth V
Post-kinematic

Figure 14